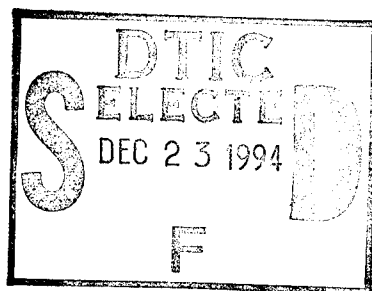


PL-TR-94-2150

Environmental Research Papers, No. 1150

**SYNTHETIC 3-D ATMOSPHERIC TEMPERATURE
STRUCTURE: A MODEL FOR KNOWN
GEOPHYSICAL POWER SPECTRA USING
A HYBRID AUTOREGRESSION AND
FOURIER TECHNIQUE**

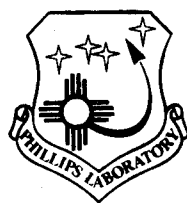
James H. Brown



25 May 1994

*Original contains color
plates: All DTIC reproduct-
ions will be in black and
white*

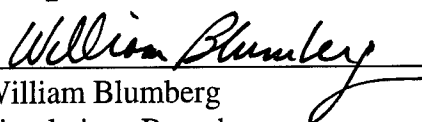
APPROVED FOR PUBLIC RELEASE; DISTRIBUTION UNLIMITED




**PHILLIPS LABORATORY
Directorate of Geophysics
AIR FORCE MATERIEL COMMAND
HANSCOM AIR FORCE BASE, MA 01731-3010**

19941219 008

"This technical report has been reviewed and is approved for publication"


William Blumberg
Simulations Branch
Branch Chief


Roger VanTassel
Optical Environment Division
Division Director

This report has been reviewed by the ESC Public Affairs Office (PA) and is releasable to the National Technical Information Service (NTIS).

Qualified requestors may obtain additional copies from the Defense Technical Information Center (DTIC). All others should apply to the National Technical Information Service (NTIS).

If your address has changed, if you wish to be removed from the mailing list, or if the addressee is no longer employed by your organization, please notify PL/TSI, 29 Randolph Road, Hanscom AFB, MA 01731-3010. This will assist us in maintaining a current mailing list.

Do not return copies of this report unless contractual obligations or notices on a specific document requires that it be returned.

REPORT DOCUMENTATION PAGE			Form 298 298	
Public reporting for this collection of information is estimated to average 1 hour per response, including the time for reviewing instructions, searching existing data sources, gathering and maintaining the data needed, and completing and reviewing the collection of information. Send comments regarding this burden estimate or any other aspect of this collection of information, including suggestions for reducing this burden, to Washington Headquarters Services, Directorate for Information Operations and Reports, 1215 Jefferson Davis Highway, Suite 1204, Arlington, VA 22202-4302, and to the Office of Management and Budget, Paperwork Reduction Project (0704-0188), Washington, DC 20503.				
1. AGENCY USE ONLY (Leave blank)		2. REPORT DATE 25 May 1994		3. REPORT TYPE AND DATES COVERED Scientific Interim (1 Oct 92-31 May 94)
4. TITLE AND SUBTITLE Synthetic 3-D Atmospheric Temperature Structure: A Model for Known Geophysical Power Spectra Using a Hybrid Autoregression and Fourier Technique			5. FUNDING NUMBERS Project: S311, 3054 Task: S31105, 3054GD WU: S3110501, 3054GD04 PE: 63215C	
6. AUTHOR(S) James H. Brown				
7. PERFORMING ORGANIZATION NAME(S) AND ADDRESS(ES) Phillips Laboratory (GPOS) 29 Randolph Road Hanscom AFB, MA 01731-3010			8. PERFORMING ORGANIZATION REPORT NUMBER PL-TR-94-2150 ERP, No. 1150	
9. SPONSORING/MONITORING AGENCY NAME(S) AND ADDRESS(ES)			10. SPONSORING/MONITORING AGENCY REPORT NUMBER	
11. SUPPLEMENTARY NOTES				
12a. DISTRIBUTION/AVAILABILITY STATEMENT Approved for public release; distribution unlimited			12b. DISTRIBUTION CODE	
13. ABSTRACT (Maximum 200 words) Geophysical phenomena are often characterized by smooth continuous power spectra having a domain of negative slope power law dependence. Frequently, Fourier transform analysis has been employed to synthesize scenes from pseudorandom arrays by passing the random samples through a Fourier filter having a desired correlation structure and power spectral dependency. This report approaches synthesis of three-dimensional synthetic structure by invoking autoregression analysis in conjunction with the Fourier method. Since computations that apply multidimensional fast Fourier transforms to large data arrays consume enormous resources, the goal of this study is to seek an alternative method to reduce the computational burden. Future releases of the Phillips Laboratory Strategic High Altitude Atmospheric Radiance Code (SHARC) will feature an ability to calculate structured radiance. The methods explored here provide a process that can complement or sometimes supplement methods presently being used. The three-dimensional temperature structure realizations generated by these methods were used to produce two-dimensional integrated temperature structure scenes that showed compliance with the input specifications.				
14. SUBJECT TERMS Power spectra, PSD, Spectral analysis, Autoregression, Fourier transform, SHARC, Structure simulation, Temperature structure, Atmospheric structure, Clutter, 3-D structure			15. NUMBER OF PAGES 54	
			16. PRICE CODE	
17. SECURITY CLASSIFICATION OF REPORT Unclassified	18. SECURITY CLASSIFICATION OF THIS PAGE Unclassified	19. SECURITY CLASSIFICATION OF ABSTRACT Unclassified	20. LIMITATION OF ABSTRACT SAR	

Accession For	
NTIS CRA&I	<input checked="" type="checkbox"/>
DTIC TAB	<input type="checkbox"/>
Unannounced	<input type="checkbox"/>
Justification	
By	
Distribution/	
Availability	
Dist	Special
A-1	

Contents

1. INTRODUCTION	1
2. GEOMETRY	3
3. AUTO-REGRESSION THEORY	5
4. PSD MODEL DISCUSSION	8
5. SIMULATION OF CORRELATED VERTICAL COMPONENTS	10
6. SIMULATION OF CORRELATED HORIZONTAL COMPONENTS	16
7. RESULTS - VALIDATION OF SIMULATED DATABASE	17
8. DATABASE	25
9. SYNTHETIC 2-D δT SCENE FOR IMITATION TEMPERATURE SENSOR	29
10. CONCLUSION	34
REFERENCES	37
APPENDIX: COMPUTATIONAL DETAILS	39

Illustrations

1. Database Geometry. Figure 1a illustrates the volume of the spherical segment defined by the database. Figure 1b illustrates the resolution volume at 50 km. 4
2. Computational Scheme. Correlations along the vertical lines are calculated (one layer at a time) and then the horizontal correlation calculation is applied to each layer. 12
3. Horizontal Correlation Lengths Plotted as a Function of Altitude. 13
4. Vertical Correlation Lengths Plotted as a Function of Altitude. 14
5. Root Mean Square Values of the Relative Temperature Fluctuations Plotted as a Function of Altitude. 15

6.	Graphs of Vertical, Transverse, and Line-of-sight One-dimensional Power Spectral Densities Plotted Against Spatial Frequency. The left panel plots the vertical PSDs for the theoretical model (light gray solid curve), autoregressive "generator" model (dashed curve), and the autoregressive vertical PSD from the simulated database (dotted curve). The middle panel plots the transverse PSDs for the theoretical model (light gray solid curve), autoregressive PSD from the simulated database (dotted curve), and a periodogram from the simulated database (solid curve). The right panel plots the line-of-sight PSDs for the theoretical model (light gray solid curve), autoregressive PSD from the simulated database (dotted curve), and a periodogram from the simulated database (solid curve).	20
7.	One-dimensional Periodograms of the First Four Samples of the Line-of-sight Simulated Data in the Layer at 50.6 km.	22
8.	Same as Figure 6 Except Altitude = 119.3 km, $\sigma^2 = 0.0277$, $L_{cv} = 2.42$ km, and $L_{ch} = 49.1$ km.	23
9.	Histogram Representing the Probability Distribution Function of the Simulated Data at 50.6 km.	26
10.	Cumulative Distribution Function of the Simulated Data at 50.6 km Compared to the Theoretical Curve.	27
11.	Sample Page From the Database Explanation File.	28
12.	Viewing Geometry of an Imaginary Temperature Sensor Platform Located at an Altitude of 85 km.	30
13.	Integrated Temperature Structure Along Selected Pixel Rows Comprising Zenith Look Angles From the Minimum of 94.6° to the Maximum of 96° .	31
14.	Integrated Temperature Structure Along Selected Pixel Columns Comprising Horizontal Look Angles From -1.07° to $+1.07^\circ$.	32
15.	Fourier Periodograms of the Horizontally Scanned Simulated Atmosphere for the Same Look Angles as Figure 13.	33
16.	PSD Estimates of the Horizontally Scanned Simulated Atmosphere from Autoregressive Analysis.	33
17.	Full Two-dimensional Integrated Temperature Structure "Scene".	35
A1.	Alias Branches of Estimated "Theoretical" LOS PSD.	41
A2.	"Theoretical" Transverse PSD Versus a 512 Point PSD "Corrected" for Truncation of the Autocorrelation Function.	45
A3.	Approximation Correction for Rectangular Window Discrete Fourier Transform Digital Sinc Function.	46

Tables

1. Database Specifications.	4
2. Correlation Lengths: Specified vs Database Estimates.	24
3. Estimated Errors, Specified Parameters vs Database Values.	25

Acknowledgment

The author gratefully acknowledges the contributions of Neil Grossbard for the computer programs, computer runs, graphics, and insights into the mathematical analysis that helped make this report possible.

Synthetic 3-D Atmospheric Temperature Structure: A Model for Known Geophysical Power Spectra Using a Hybrid Autoregression and Fourier Technique

1. INTRODUCTION

Atmospheric fluctuations in wind speed, temperature, and density are characterized by continuous power spectral density functions. For example, one-dimensional horizontal wind speed PSDs are found to have horizontal wavenumber log-log slopes of about $-5/3$ and vertical wavenumber log-log slopes of -3 . Such spectra, parameterized by spectral slope, correlation lengths, and moments of probability density functions, are often used in simulating an environment or predicting atmospheric structure. Multidimensional fast Fourier transform synthesis provides a means for filtering white noise with spatial filters to simulate a stationary time or spatial data set. Autoregression synthesis provides a fast means for simulating a one-dimensional *non-stationary* spatial structure sequence.

The Phillips Laboratory Strategic High Altitude Atmospheric Radiance Code (SHARC)¹ uses first principles to calculate point to space and limb viewing atmospheric background infrared (IR) radiance and transmittance under both local-thermal-equilibrium (LTE) and non-local-

(Received for publication 14 June 1994)

¹ Sharma, R.D., Duff, J.W., Sundberg, R.L., Gruninger, J.H., Bernstein, L.S., Robertson, D.C., and Healey, R.J. (1991) *Description of SHARC-2, The Strategic High Altitude Atmospheric Radiance Code*, Phillips Laboratory Tech. Rpt., PL-TR-91-2071. ADA239008

thermal-equilibrium (NLTE) conditions above 50 km. Release 3 of the SHARC code² predicts IR radiation and transmittance in the 1-40 μm spectral region and includes important bands from the major isotopes of NO, CO, H₂O, O₃, OH, CO₂, CH₄, and NO⁺. Specific local atmospheric environments can be specified through region definitions, and diurnal characteristics can be specified through user or program generated multiple vertical concentration profiles. A subroutine module breaks a given line-of-sight (LOS) specification into small segments and determines the composition and properties of each segment. Each segment is determined by the intersection of the LOS with an altitude layer boundary, defined in input atmospheric profiles. Appropriate profiles of temperature, pressure, and molecular state densities are determined for each segment.

A future release of SHARC will have the ability to provide realizations of atmospheric infrared volume-emission perturbations that occur from fluctuations in temperature and density of the contributing molecular species. Version 4 of the SHARC code envisions a capability to evaluate radiance structure from estimated variances in the standard temperature and density profiles. The algorithms will simulate IR fluctuations that must depend on relatively small fluctuations in atmospheric species number densities, vibrational state populations, and the kinetic temperatures along a given line-of-sight.^{3,4} Where NLTE effects dominate, (generally above 50 km) a small fluctuation in kinetic temperature can produce correlated changes, anti-correlated changes, or no change in the vibrational state temperature. Such changes ultimately depend on the relative contributions from total number density, temperature-dependent kinetic rates, and radiative relaxation. A proper description of the temperature/density field is thus needed to enable SHARC to correctly compute the radiance structure field.

To provide a realistic but practical two-dimensional structure scene capability requires creative, efficient, and tested algorithms. This report presents a method of producing stochastic three dimensional *non-stationary* synthetic spatial structure from a hybrid one-dimensional (vertical) autoregressive component and a two-dimensional (horizontal) Fourier

² Gruninger, J., Sundberg, R.L., Duff, J.W., Bernstein, L.S., Matthew, M.W., Adler-Golden, S., Robertson, D., Sharma, R., Brown, J.H., Healey, R., and Vail J. (1994) SHARC - 3, A model for infrared radiance at high altitudes, *Proc. SPIE - The International Society of Optical Engineering*, V:2223, Orlando, Florida.

³ Sundberg, R.L., Gruninger, J., De, P., Brown, J.H. (1994) Infrared radiance fluctuations in the upper atmosphere, *Proc. SPIE - The International Society of Optical Engineering*, V:2223, Orlando, Florida.

⁴ Sears, R.D., Strugala, L.A., Newt, J., Robertson, D., Brown, J.H., and Sharma, R. (1994) Simulation of the infrared structured earthlimb background using the SHARC radiance code, 32nd Aerospace Sciences Meeting and Exhibit, Reno, NV.

transform component. In this report we extend the results expressed in two previous reports that dealt with one-dimensional autoregression⁵ and two-dimensional autoregression/moving average⁶ structure simulation.

2. GEOMETRY

SHARC is capable of predicting earthlimb radiance along a sensor line-of-sight (LOS) as a function of LOS and tangent altitude. In this report, temperature and density perturbations are incorporated on the mean atmosphere to enable SHARC calculations of stochastic radiance structure. An appropriately configured three-dimensional database of stochastic temperature structure is needed. To fill this need, the non-stationary database has been developed in a three-dimensional matrix that is described geometrically by a segment of a sphere. The spherical segment consists of a volume 70 km in radial height by approximately 3000 km long by approximately 51.2 km wide. The horizontal matrix elements lie in a spherical surface at radial distance "r". Since we wish the database (that is, the synthetic atmosphere) to be applicable for observation by a modeled sensor, we orient the longer horizontal dimension along the sensor LOS direction and the shorter horizontal dimension along the direction transverse to the line-of-sight. The spatial resolution of a matrix element has an incremental altitude of 0.1 km by an incremental transverse distance of approximately 0.1 km by an incremental LOS distance of approximately 15.7 km. Thus, the database matrix consists of 701 vertical elements aligned along radial lines, 512 transverse horizontal elements, and 192 line-of-sight horizontal elements. The actual data spacing in the horizontal dimension must increase slightly with altitude so that points in the vertical dimension stay on radial lines. The altitude range accounts for dominant structure effects (50-120 km). Also its vertical and transverse dimensions are sufficient to fill the field of a limb-viewing two-dimensional sensor array. The vertical and transverse spatial resolution are governed by the vertical and horizontal correlation lengths of the temperature variations but also are chosen to provide high field-of-view spatial resolution. The geometrical LOS dimensions are chosen to provide sufficient length to describe the integrated path radiance. Figure 1 illustrates the spherical geometry and Table 1 summarizes the database specifications.

⁵ Brown, J.H. (1993) *Atmospheric Structure Simulation: An Autoregressive Model for Smooth Geophysical Power Spectra with Known Autocorrelation Function*, Phillips Laboratory Tech. Rpt., PL-TR-93-2185, ERP No. 1128, ADA 276691.

⁶ Brown, J.H. (1993) *Atmospheric Structure Simulation: An ARMA Model for Smooth Isotropic Two-Dimensional Geophysical Power Spectra*, Phillips Laboratory Tech. Rpt., PL-TR-93-2224, ERP No. 1132, ADA 280476.

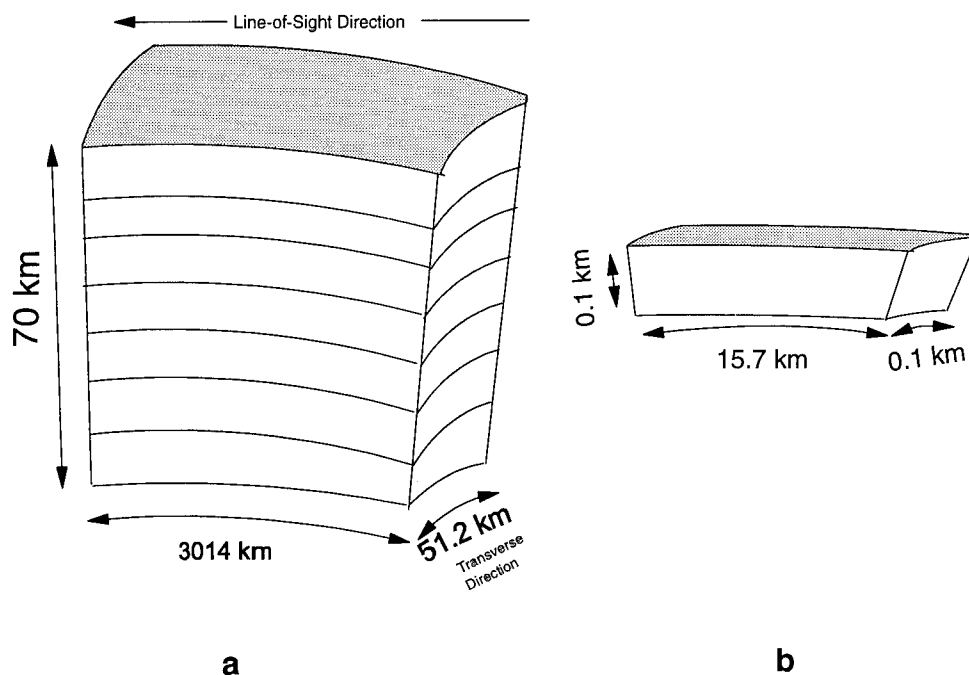


Figure 1. Database Geometry. Figure 1a illustrates the volume of the spherical segment defined by the database. The radial altitude range starts at 50 km and ends at 120 km. At 50 km altitude the curved length in the LOS direction measures 3014 km while the curved length in the transverse direction measures 51.2 km. These distances increase slightly with altitude due to the curved geometry. Figure 1b illustrates the resolution volume at 50 km. The radial altitude resolution is 0.1 km while the resolution of the curved lengths in the LOS and transverse directions is 15.7 km and 0.1 km respectively. Again the horizontal resolution lengths increase slightly with altitude.

Table 1. Database Specifications

Direction	N pts	Δx (km)	N Δx (km)	freq. res. $1/N \Delta x$ (cy/km)	Nyquist freq. $1/2 \Delta x$ (cy/km)
Vertical (50-120 km)	700	0.1	70	---	---
Transverse	512	0.1	51.2	0.0195 (HIGH)	5
LOS	192	15.7	3014.	0.00033	0.0318 (LOW)

3. AUTO-REGRESSION THEORY

This section briefly reviews autoregressive digital spectral estimation as presented by S. Lawrence Marple⁷ and Steven M. Kay.⁸

An autoregressive moving average (ARMA) model for a discrete spatial series $v(n)$, that approximates deterministic and stochastic processes can be represented by the filter linear difference equation:

$$v(n) = - \sum_{j=1}^p a(j) v(n-j) + \sum_{j=0}^q b(j) \varepsilon(n-j)$$

in which $v(n)$ is the output sequence and $\varepsilon(n)$ a white noise input driving sequence. The $a(j)$ and $b(j)$ coefficients form the autoregressive and moving average portions of the ARMA model respectively. A z-transform analysis of the difference equation shows that the ARMA power spectral density ($P_{ARMA}(k)$) is:

$$P_{ARMA}(k) = \Delta v \sigma_w^2 \left| \frac{B(k)}{A(k)} \right|^2 \quad \text{for } -\infty \leq k \leq \infty$$

where k is the spatial frequency and where,

$$A(k) = 1 + \sum_{j=1}^p a(j) \exp(-2\pi i k j \Delta v)$$

and,

$$B(k) = 1 + \sum_{j=1}^q b(j) \exp(-2\pi i k j \Delta v), \text{ with } b(0) = 1.$$

⁷ Marple, S.L. (1987) *Digital Spectral Analysis with Applications*, Chapter 6, Prentice-Hall, Englewood, New Jersey.

⁸ Kay, Steven M. (1988) *Modern Spectral Estimation, Theory & Application*, Prentice-Hall, Englewood, New Jersey.

Here Δv is the sampling interval, σ_w^2 is the variance of the white noise process, and $i = \sqrt{-1}$. If all the moving average coefficients are zero, except $b(0) = 1$, then,

$$v(n) = - \sum_{j=1}^p a(j)v(n-j) + \varepsilon(n)$$

and the process is strictly autoregressive of order p . The autoregressive PSD becomes:

$$P_{AR}(k) = \frac{2\Delta v \sigma_w^2}{|A(k)|^2} = 2\Delta v \sum_{j=-\infty}^{\infty} r_{vv}(j) \exp(-2\pi i k j \Delta v), \text{ for } 0 \leq k \leq \infty$$

where r_{vv} is the real and even autocorrelation sequence at j , and σ_w^2 is the variance of $\varepsilon(n)$. The relationship between the autocorrelation sequence and the pure autoregressive model is:

$$r_{vv}(m) = \begin{cases} - \sum_{j=1}^p a(j)r_{vv}(m-j) & \text{for } m > 0 \\ - \sum_{j=1}^p a(j)r_{vv}(-j) + \sigma_w^2 & \text{for } m = 0 \\ r_{vv}^*(-m) & \text{for } m < 0 \end{cases}$$

This expression may be evaluated for the $p+1$ lag indices $0 \leq m \leq p$ by:

$$\begin{pmatrix} r_{vv}(0) & r_{vv}(-1) & \dots & r_{vv}(-p) \\ r_{vv}(1) & r_{vv}(0) & \dots & r_{vv}(-p+1) \\ \vdots & \vdots & \ddots & \vdots \\ r_{vv}(p) & r_{vv}(p-1) & \dots & r_{vv}(0) \end{pmatrix} \begin{pmatrix} 1 \\ a(1) \\ \vdots \\ a(p) \end{pmatrix} = \begin{pmatrix} \sigma_w^2 \\ 0 \\ \vdots \\ 0 \end{pmatrix}$$

This expression forms the autoregressive Yule-Walker equations. Given the autocorrelation sequence for lags 0 to p , the autoregressive coefficients may be found from the above. Since $r_{vv}(-k) = r_{vv}^*(k)$, the autocorrelation matrix is both Toeplitz and Hermitian. A standard "Levinson" algorithm that takes advantage of the Hermitian-Toeplitz matrix equation was employed to solve for the AR parameters. The same Yule-Walker equations also occur if we attempt to solve the problem: find the "best", in a least square sense, set of equations that determine the coefficients that predict \hat{v} from $\hat{v}(n) = - \sum_{j=1}^p a(j)v(n-j)$, where

$$\overline{(\hat{v}(n) - v(n))^2} = \sigma_w^2. \text{ In summary, the Levinson recursion computes sets of coefficients}$$

$$\{a_1(1), \sigma_1^2\}, \{a_2(1), a_2(2), \sigma_2^2\}, \dots, \{a_p(1), a_p(2), \dots, a_p(p), \sigma_p^2\}$$

where the final set at order p is the desired solution of the Yule-Walker expressions. For the AR(p) process, $a_p(j) = a(j)$ for $j = 1, 2, 3, \dots, p$ and σ_p^2 is the minimum prediction error, that is, $\sigma_p^2 = \sigma_w^2 = \sigma_{\min}^2 = \xi[v^*[n](v[n]) - \hat{v}[n]]$. The algorithm is initialized by:

$$a_1[1] = - \frac{r_{vv}[1]}{r_{vv}[0]}$$

$$\sigma_1^2 = (1 - |a_1[1]|^2) r_{vv}[0]$$

with the recursion for $j = 2, 3, \dots, p$ given by:

$$a_j[j] = - \frac{r_{vv}[j] + \sum_{\mu=1}^{j-1} a_{j-1}[\mu] r_{vv}[j-\mu]}{\sigma_{j-1}^2}$$

$$a_j[\eta] = a_{j-1}[\eta] + a_j[j] a_{j-1}^*[j-\eta] \quad \eta = 1, 2, \dots, j-1$$

$$\sigma_j^2 = (1 - |a_j[j]|^2) \sigma_{j-1}^2.$$

The $a_j[j]$ coefficients are known as reflection coefficients.

4. PSD MODEL DISCUSSION

Atmospheric power spectral density functions often are modeled by isotropic one-dimensional double-sided power law functions of the form:^{9,10}

$$PSD(k) = \frac{C}{(a^2 + k^2)^{v+\frac{1}{2}}}, \quad \text{for } -\infty \leq k \leq \infty.$$

The constant C is found from the definition that the total variance of the associated time series, σ^2 , is equal to the area under the PSD:¹¹

$$\sigma^2 = 2 \int_0^\infty PSD(k) dk = 2C \int_0^\infty \frac{dk}{(a^2 + k^2)^{v+\frac{1}{2}}} = 2C \frac{\sqrt{\pi} \Gamma(v)}{2a^{2v} \Gamma\left(v + \frac{1}{2}\right)}$$

so that the three-parameter one-dimensional PSD model is:

$$PSD(k) = \frac{a^2 a^{2v} \Gamma\left(v + \frac{1}{2}\right)}{\sqrt{\pi} \Gamma(v) (a^2 + k^2)^{v+\frac{1}{2}}}.$$

⁹ Tatarski, V.I. (1961) *Wave Propagation in a Turbulent Medium*, McGraw-Hill.

¹⁰ Futterman, W.I., Schweitzer, E.L., and Newt, J.E. (1991) Estimation of scene correlation lengths, characterization, propagation, and simulation of sources and backgrounds, *Proc. SPIE - The International Society of Optical Engineering*, V:1486, pp127-140, Orlando, Florida.

¹¹ For the integral, see for example, Gradshteyn, I.S. and Ryzhik, I.M. (1965) *Table of Integrals Series and Products*, eq 3.241.4, Academic Press.

The relationship between the frequency domain *PSD* and the time or spatial domain autocorrelation function is specified by their Fourier transform pairs. Thus the autocorrelation function, (*ACF*), for the real even *PSD* function is:

$$ACF(x) = IFFT(PSD) = 2 \int_0^{\infty} \frac{\sigma^2 \Gamma\left(v + \frac{1}{2}\right) a^{2v} \cos(2\pi x k) dk}{\sqrt{\pi} \Gamma(v) (a^2 + k^2)^{v + \frac{1}{2}}}.$$

The integral is solved in terms of the Bessel function of the second kind of fractional order, K_v , as:¹²

$$ACF(x) = \frac{\sigma^2 2^{(1-v)} (2\pi a x)^v K_v(2\pi a x)}{\Gamma(v)}.$$

The parameter " a " can be expressed in terms of the integral scale or equivalent width, L , of the autocorrelation function. An equivalent width is defined as the area of a function divided by its central ordinate,¹³ or,

$$L = \frac{\int_0^{\infty} f(x) dx}{f(0)}.$$

Thus the large scale correlation length L_c is defined by integrating $ACF(x)$ over all positive values of x .

$$L_c = \frac{\int_0^{\infty} ACF(x) dx}{\sigma^2},$$

¹² Gradshteyn, I.S. and Ryzhik, I.M. (1965) *Table of Integrals Series and Products*, eq 8.432.5, Academic Press.

¹³ Bracewell, R.N. (1978) *The Fourier Transform and Its Applications*, McGraw-Hill, New York.

where σ^2 is the autocorrelation at zero separation. Since

$\int_0^\infty ACF(x) dx = \frac{1}{2} \int_{-\infty}^\infty ACF(x) dx \frac{1}{2} = PSD(0)$ and $ACF(0) = \sigma^2$, the equivalent width or correlation length as a function of the PSD may also be written as:

$$L_c = \frac{PSD(0)/2}{\int_{-\infty}^\infty PSD(k) dk} = \frac{PSD(0)}{2\sigma^2}$$

so that,

$$L_c = \frac{\sigma^2 \Gamma\left(v + \frac{1}{2}\right) a^{2v}}{2\sigma^2 \sqrt{\pi} \Gamma(v) a^{2v+1}} = \frac{\Gamma\left(v + \frac{1}{2}\right)}{2\sqrt{\pi} \Gamma(v) a} \text{ or}$$

$$a^{-1} = \frac{2\sqrt{\pi} \Gamma(v)}{\Gamma\left(v + \frac{1}{2}\right)} L_c.$$

5. SIMULATION OF CORRELATED VERTICAL COMPONENTS

In practice, a given one-dimensional *single-sided* PSD was constructed from the PSD and ACF power law models:

$$PSD(k) = \frac{2\sigma_r^2 a^{2v} \Gamma\left(v + \frac{1}{2}\right)}{\sqrt{\pi} \Gamma(v) (a^2 + k^2)^{v + \frac{1}{2}}} \approx \frac{2\sigma_r^2 \Delta v}{\left|1 + \sum_{j=1}^N a_j e^{i2\pi k \Delta v}\right|^2}, \text{ for } 0 \leq k \leq \infty$$

$$ACF(v) = \frac{\sigma^2 2^{(1-v)} (2\pi a v)^v K_v(2\pi a v)}{\Gamma(v)}$$

where,

$\sigma_r^2 \equiv$ residual error
 $v \equiv$ vertical distance
 $\Delta v \equiv$ vertical spacing
 $a_j \equiv$ model parameters
 $i \equiv \sqrt{-1}$
 $k \equiv$ frequency (km^{-1})

Conceptually, radial line segments having an origin at the center of the earth define a segment of a sphere. Along the geometrical set of these radial or vertical line segments, a spatial data sequence was simulated using a normally distributed set of pseudorandom numbers $G(J)$. In this case, there were 512×192 independent sets of random numbers corresponding to vertical elements along the radial lines. The sequence, $G(J)$, was initialized by an arbitrary seed and thus the set of random numbers differed for each line. $G(J)$ consisted of a mean equal to zero and variance equal to 1. The simulation of 701 sequence values along each vertical (radial) line was generated from six autoregression coefficients by the expression:

$$Y(J) = G(J) - \sum_{j=1}^6 a_j Y(J-j) \text{ where the } a_j \text{ values were determined from the previously described}$$

Levinson algorithm. Note that the first level of non-stationarity is built into the database by allowing the a_j values to dynamically change with altitude as a function of the vertical correlation length. The first 51 values of $Y(J)$ for each radial line were discarded to allow for filter relaxation. In practice, for altitudes above 50 km, the calculational scheme stepped along at each altitude layer. First the vertically correlated component for a particular layer (the top layer in the array) was computed with $\sigma^2 = 1$. The layer was then copied to a second array where the appropriate horizontal correlation and σ^2 were applied for that layer. Since σ^2 and horizontal correlation length change with altitude, these parameters were applied to the horizontal layer in the copied array to account for the second level of non-stationarity. Thus each layer in the copied array contained both the vertical and horizontal correlations before the computations proceeded to the next higher layer. The scheme is represented in Figure 2.

The altitude dependence of the relative temperature variance, horizontal correlation length, and vertical correlation length are adopted from Strugala, et.al.^{14,15} Their values and our fitted models of them are shown in Figures 3-5. Logistic dose response equations were used in fitting the data. The outside curves in each graph represent the 95 percent confidence limits. The fitted curves were used to evaluate the parameters as a function of altitude.

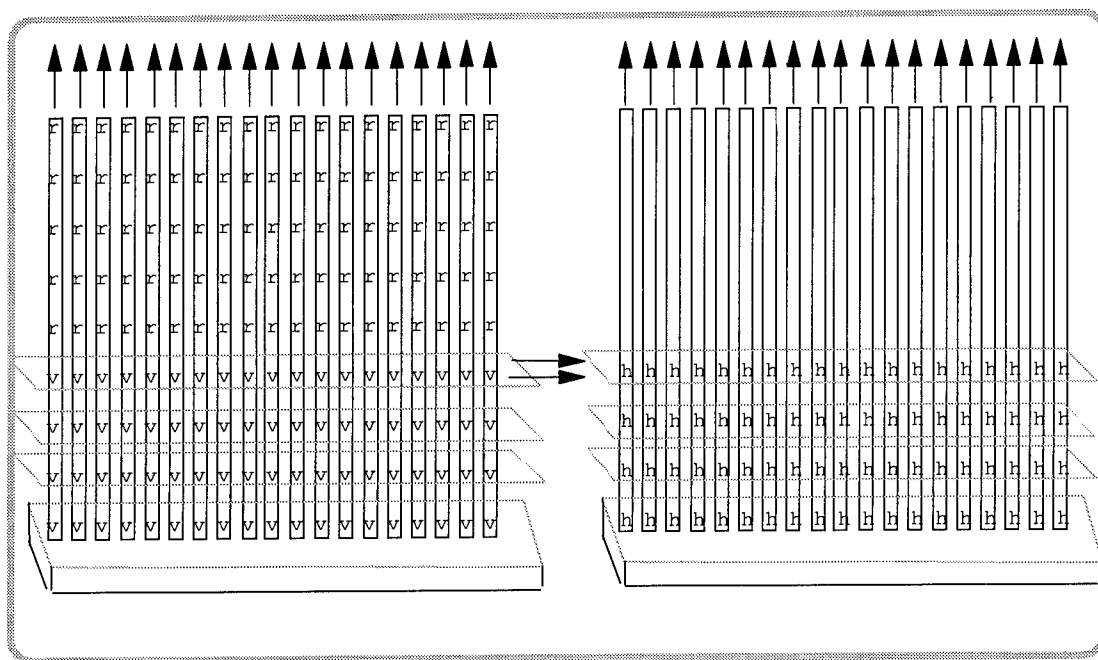
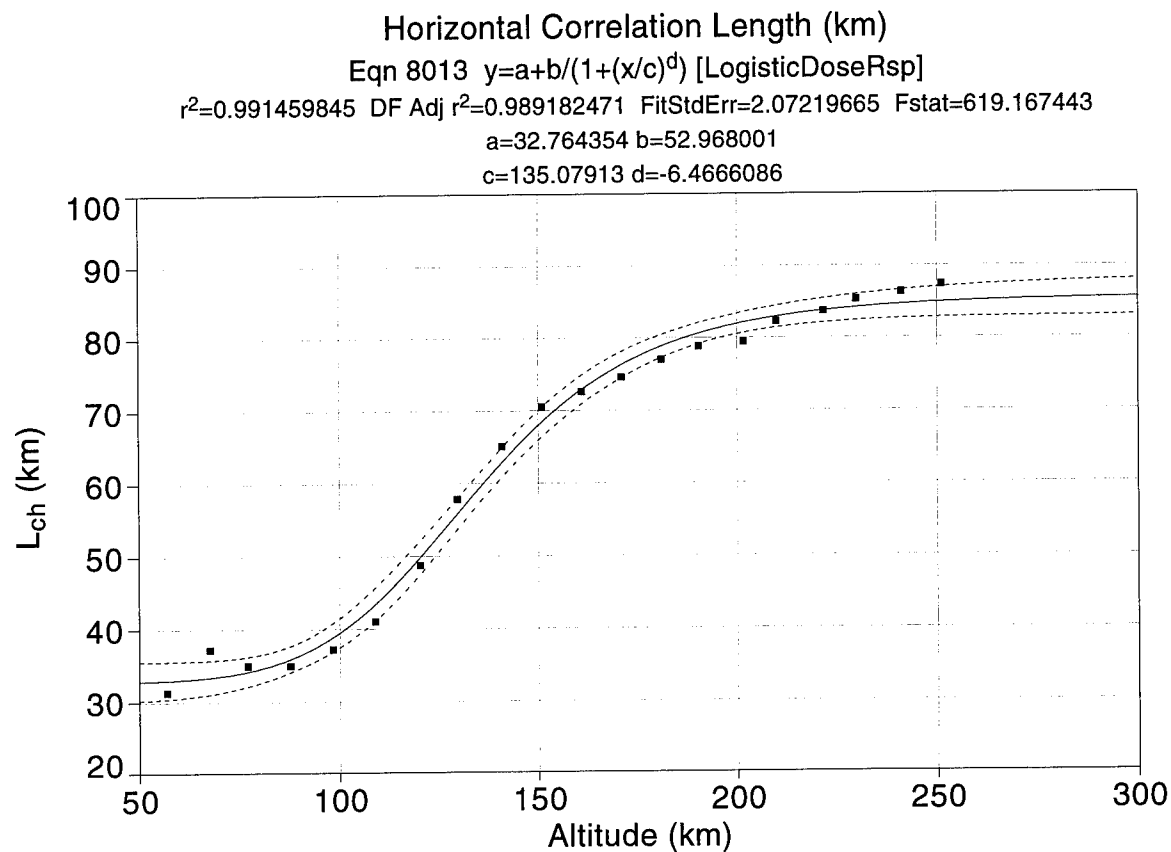


Figure 2. Computational Scheme. First, correlations along the vertical lines are calculated (one layer at a time) and then the horizontal correlation calculation is applied to each layer.

¹⁴ Strugala, L.A. (1991) Development of high resolution statistically non-stationary infrared earthlimb radiance scenes, characterization, propagation, and simulation of sources and backgrounds, *Proc. SPIE - The International Society for Optical Engineering*, **V**:1486, pp. 176-187, Orlando, Florida.

¹⁵ Strugala, L.A. (1993) Production of statistically nonstationary stochastic structure realizations for infrared background scene simulations, *Optical Engineering*, **V32**(No. 5):, pp. 993-1001.

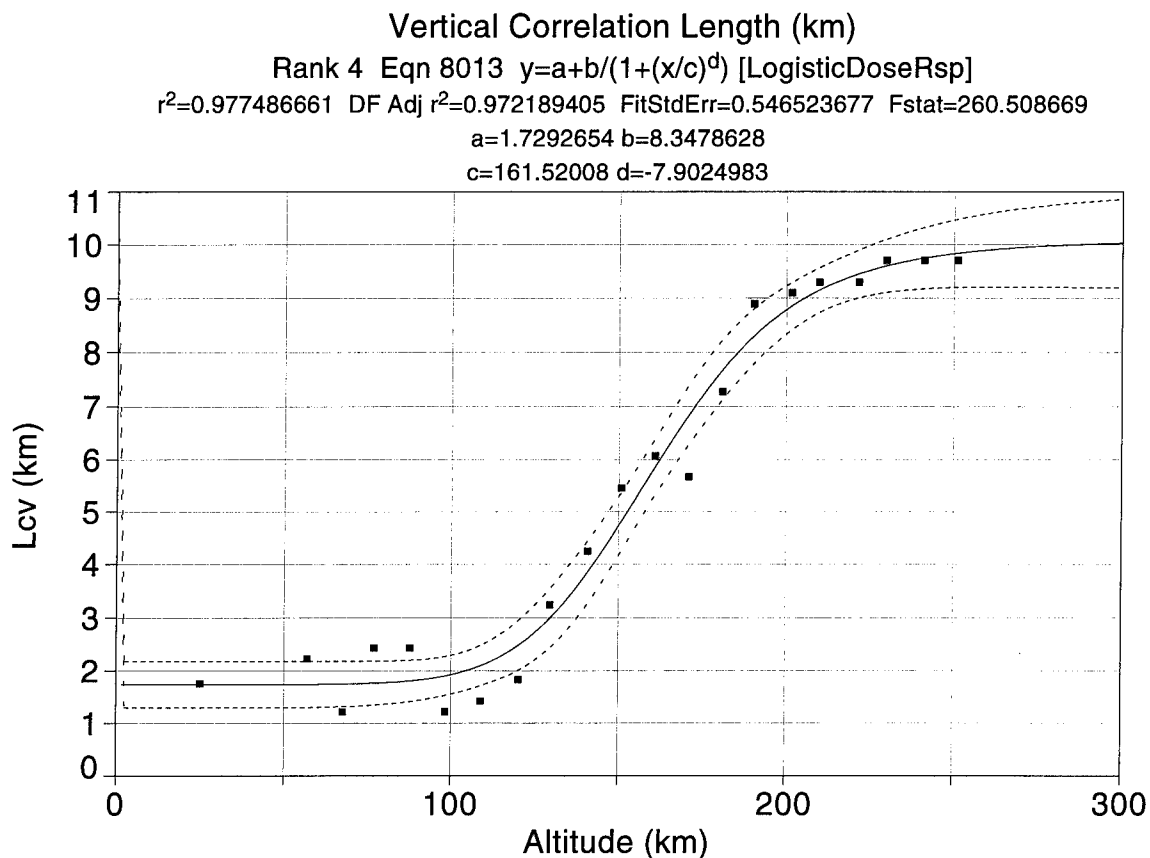


Rank 18 Eqn 8013 $y=a+b/(1+(x/c)^d)$ [LogisticDoseRsp]

r^2	Coef Det	DF Adj r^2	Fit Std Err	F-value
0.9914598452		0.9891824705	2.0721966466	619.16744310

Parm	Value	Std Error	t-value	95% Confidence Limits	
a	32.76435426	1.295628218	25.28839199	30.01210311	35.51660541
b	52.96800100	2.144297606	24.70179552	48.41295545	57.52304655
c	135.0791315	2.234742679	60.44504933	130.3319571	139.8263059
d	-6.46660858	0.680074818	-9.50867230	-7.91126428	-5.02195287

Figure 3. Horizontal Correlation Lengths Plotted as a Function of Altitude. A logistic dose response equation is fitted to the data. The outside curves represent the 95 percent confidence limits.

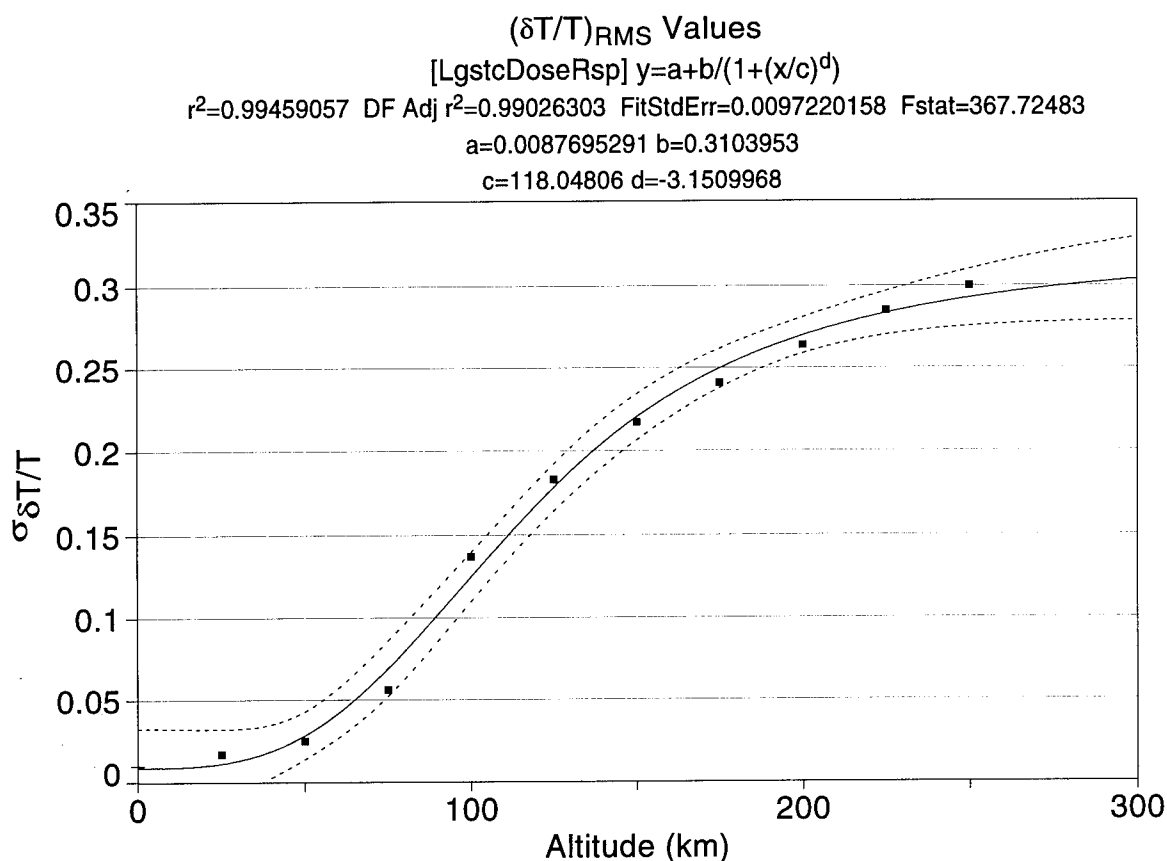


Rank 4 Eqn 8013 $y=a+b/(1+(x/c)^d)$ [LogisticDoseRsp]

r^2	Coef Det	DF Adj r^2	Fit Std Err	F-value
0.9774866610		0.9721894048	0.5465236769	260.50866885

Parm	Value	Std Error	t-value	95% Confidence Limits	
a	1.729265412	0.210585414	8.211705540	1.286422835	2.172107988
b	8.347862811	0.536310568	15.56535207	7.220048927	9.475676694
c	161.5200848	3.853308016	41.91725244	153.4169175	169.6232522
d	-7.90249825	1.339177504	-5.90100881	-10.7186706	-5.08632592

Figure 4. Vertical Correlation Lengths Plotted as a Function of Altitude. A logistic dose response equation is fitted to the data. The outside curves represent the 95 percent confidence limits.



Rank 931 Eqn 8013 [LgstcDoseRsp] $y=a+b/(1+(x/c)^d)$

r^2 Coef Det	DF Adj r^2	Fit Std Err	F-value
0.9945905715	0.9902630287	0.0097220158	367.72482563

Parm	Value	Std Error	t-value	95% Confidence Limits	
a	0.008769529	0.009675816	0.906334825	-0.01500493	0.032543990
b	0.310395297	0.024196036	12.82835344	0.250943187	0.369847408
c	118.0480550	5.745293881	20.54691326	103.9312859	132.1648241
d	-3.15099683	0.473460616	-6.65524591	-4.31433753	-1.98765613

Date	Time	File Source
Jun 1, 1994	10:59:59 AM	d:\tcwin2\rms1.prn

Figure 5. Root Mean Square Values of the Relative Temperature Fluctuations Plotted as a Function of Altitude. A logistic dose response equation is fitted to the data. The outside curves represent the 95 percent confidence limits.

After simulating the vertical spatial sequences of a given *PSD*, the *PSD* of the simulated vertical series was checked using a forward and backward estimation method.¹⁶ A set of 6 b_j coefficients were found to estimate the simulated *PSD* from the formula,

$$PSD_{est}(k) = \frac{2\sigma_c^2 \Delta v}{\left| 1 + \sum_{j=1}^6 b_j e^{i2\pi k \Delta v} \right|^2},$$

where σ_c^2 is described below and where Δv is the same spacing used to generate the synthetic series (0.1 km).

For a given altitude, the forward and backward method solves the following least squares problem. Given 13 discrete vertical series values $Y(J)$, for $J = 1, 2, \dots, 13$, and where $J=7$ is the layer in question, we find b_j values that minimize *ERR*, where,

$$ERR = \left(\sum_{J=7}^{13} \left(Y(J) - \sum_{j=1}^6 b_j Y(J-j) \right)^2 \right) + \left(\sum_{J=1}^7 \left(Y(J) - \sum_{j=1}^6 b_j Y(J+j) \right)^2 \right).$$

Then σ_c^2 is equal to $\frac{ERR}{14}$. In practice, *ERR* was minimized by combining the $Y(J)$ values for all vertical lines.

6. SIMULATION OF CORRELATED HORIZONTAL COMPONENTS

As discussed above, the correlations in the horizontal LOS direction, ℓ , and transverse direction, t , were applied to the previous vertically correlated simulated data by using two-dimensional Fourier transform synthesis. The model autocorrelation function used in this report leads to an isotropic two-dimensional power spectral density function given by:

¹⁶ Haykin, Simon, ed. (1991) *Advances in Spectrum Analysis and Array Processing*, V1, Prentice Hall, Englewood Cliffs, New Jersey, pp.155-156.

$$P(k_{t,\ell}) = \frac{\sigma^2 \nu a^{2\nu}}{\pi(a^2 + k_t^2 + k_\ell^2)^{\nu+1}}, \text{ for } -\infty \leq k_t, k_\ell \leq \infty.$$

This representation replaces the one-dimensional $-(2\nu+1)$ power dependence with a two-dimensional $-(2\nu+2)$ power dependence. $P(k_{t,\ell})$ was used to filter the vertically correlated Gaussian random values at a given altitude. First, the procedure found the two-dimensional Fast Fourier Transform of the two-dimensional Gaussian correlated values at a given altitude. These spatial frequency values then were multiplied by the filter function $\sqrt{P(k_t, k_\ell) / \Delta t \Delta \ell}$. A two-dimensional inverse Fourier Transform of the result gave the final correlated simulated data at the given altitude. The process stepped up in altitude to yield the three-dimensional database. Summarizing, the simulated data, $S(t, \ell)$, for a layer is described by:

$$S(t, \ell) = FFT^{-1} \left(\sqrt{\frac{P_{theor}(k_t, k_\ell)}{\Delta t \Delta \ell}} \right) \times FFT(\tilde{G}(\epsilon_t, \epsilon_\ell)), \text{ where } \tilde{G}(\epsilon_t, \epsilon_\ell) \text{ are the vertically correlated}$$

simulated data for the layer. As explained in the appendix, sampling theory results caused us to modify the expression for $S(t, \ell)$.

7. RESULTS - VALIDATION OF SIMULATED DATABASE

A practical and efficient three-dimensional non-stationary stochastic model of atmospheric structure consistent with having pre-assigned vertical and horizontal power spectral densities and autocorrelation functions is desired. In this section, we examine and compare the prescribed structure to that obtained from the stochastic hybrid method described earlier. This examination serves to validate the database. Correlation lengths and σ^2 variances were taken from the data of Strugala, et.al.¹⁴ As discussed above, fitted forms of these data were used as inputs to the autoregressive and Fourier transform filters.

First, we examine the power spectral densities of the vertical structure as depicted in the left panel of Figure 6. The light gray solid curve depicts a one-dimensional "theoretical" vertical PSD plotted against wavenumber for an altitude of 50.6 km. This figure is typical of the graphs in this section that show log-log plots of PSDs measured in

$\frac{(\delta \text{ temperature} / \text{temperature})^2}{\text{wavenumber}}$ and wavenumber measured in km^{-1} . At 50.6 km the input

parameters have a vertical correlation length $L_{cv} = 1.72$ km and a vertical spectral slope $(S) = -5/3$. The constant vertical data spacing was 0.1 km. This curve may be compared with the PSD of the AR model that was used to generate the vertically simulated data and with the PSD of the simulated data itself. The dashed curve in this plot shows the one-dimensional vertical PSD of the autoregressive model that was used at the 50.6 km altitude. In applying the autoregressive model, the variance, σ^2 , was normalized to a value of 1. The actual variance

was introduced into the synthesis during the horizontal computations. A 6-coefficient model was used to calculate or "predict" the next vertically correlated data point for the next higher layer. Points in the layer were computed by applying the autoregressive model to each vertical line in the array. Shown on the same plot is the *PSD* computed from the vertically constructed data around 50.6 km altitude. This *PSD* results from computing a 6-coefficient forward and backward autoregressive model of the vertically simulated data from layers extending from 50.0 km to 50.6 km in the forward direction and layers extending from 51.2 km to 50.6 km in the backward direction. Comparison of the curves show excellent agreement between the prescribed *PSD* and the *PSD* computed from the synthetic vertical data.

We now examine the horizontal transverse structure as depicted in the center panel of Figure 6. A light gray solid curve depicts a one-dimensional "theoretical" transverse horizontal *PSD* plotted against wavenumber for an altitude of 50.6 km. The transverse direction is perpendicular to the line-of-sight direction and the transverse data spacing is approximately 0.100 km. At 50.6 km the input parameters have a horizontal correlation length $L_{ch} = 32.9$ km, and the variance of the relative temperature fluctuations $\sigma^2 = 8.34 \times 10^{-4}$. The figure represents the 1-D component of the 2-D horizontal *PSD* having a high frequency horizontal spectral slope (S) = -8/3. This curve may be compared with a periodogram of the simulated data aligned in the layer along the transverse direction. It may also be compared with a *PSD* computed from an AR model of that same data. The solid curve in this panel shows a one-dimensional periodogram of the transverse simulated data in the layer at 50.6 km. The periodogram has a Nyquist frequency of approximately $1/(2 \times 0.1) = 5 \text{ km}^{-1}$. The periodogram was computed by averaging the individual periodograms of the simulated data along each of the 192 transverse lines in the layer. Comparison of the gray and solid curves shows excellent agreement between the prescribed *PSD* and the periodogram computed from the synthetic transverse data. The dotted curve in this panel shows another one-dimensional transverse *PSD* plotted against wavenumber for 50.6 km altitude. The curve results from computing a 10-coefficient autoregressive model of the transverse simulated data in the layer at 50.6 km. Comparison of the gray and dotted curves again shows excellent agreement between the prescribed *PSD* and the *PSD* computed from the synthetic transverse data.

Next, we examine the horizontal line-of-sight structure as depicted in the right panel of Figure 6. A light gray solid curve depicts a one-dimensional theoretically aliased line-of-sight (LOS) horizontal *PSD* plotted against wavenumber for an altitude of 50.6 km. For a detailed discussion of the aliasing issue the reader is referred to the appendix. The LOS data spacing is approximately 15.7 km. The curve represents the 1-D component of the 2-D horizontal *PSD* having a horizontal spectral slope (S) = -8/3. This figure may be used for comparison with a periodogram of the simulated data aligned in the layer along the line-of-sight direction. It may also be used for comparison with a *PSD* computed from an AR model of that same data. The solid curve in this panel shows a one-dimensional periodogram of the line-of-sight simulated data in the layer at 50.6 km. The periodogram has a Nyquist frequency of approximately $1/(2 \times 15.7) = 0.032 \text{ km}^{-1}$. The periodogram was computed by averaging the individual periodograms of the simulated data along each of the 512 LOS lines in the layer. Comparison of the gray and solid curves shows excellent agreement between the prescribed *PSD* and the mean of the periodogram computed from the synthetic transverse data. The reason for the

"noisy" PSD is the high degree of correlation between neighboring and nearby data points. This is illustrated in Figure 7, which shows the PSDs of simulated data in the layer along the first four lines along the LOS. The small differences between the PSDs are due to the high degree of correlation between data in adjacent lines. The dotted curve in the right panel of Figure 6 shows another one-dimensional line-of-sight PSD plotted against wavenumber for 50.6 km altitude. This curve results from computing a 10-coefficient autoregressive model of the line-of-sight simulated data in the layer at 50.6 km. Comparison of gray and dotted curves again shows excellent agreement between the prescribed PSD and the PSD computed from the synthetic line-of-sight data.

Power spectral density computations for 119.3 km altitude are shown in Figure 8. The graph repeats Figure 6 except that the input parameters are altitude = 119.3 km, $\sigma^2 = 0.0277$, $L_{cv} = 2.42$ km, and $L_{ch} = 49.1$ km. The transverse spacing is 0.101 km and LOS spacing is 15.9 km. Comparison with Figure 6 indicates that the hybrid method described herein may be employed for a wide range of altitudes. Additionally, -3 spectral slope models have been run with results very similar to the -5/3 spectral slope. That is, the power law dependence and PSD amplitudes specified by the models are preserved in the simulated data.

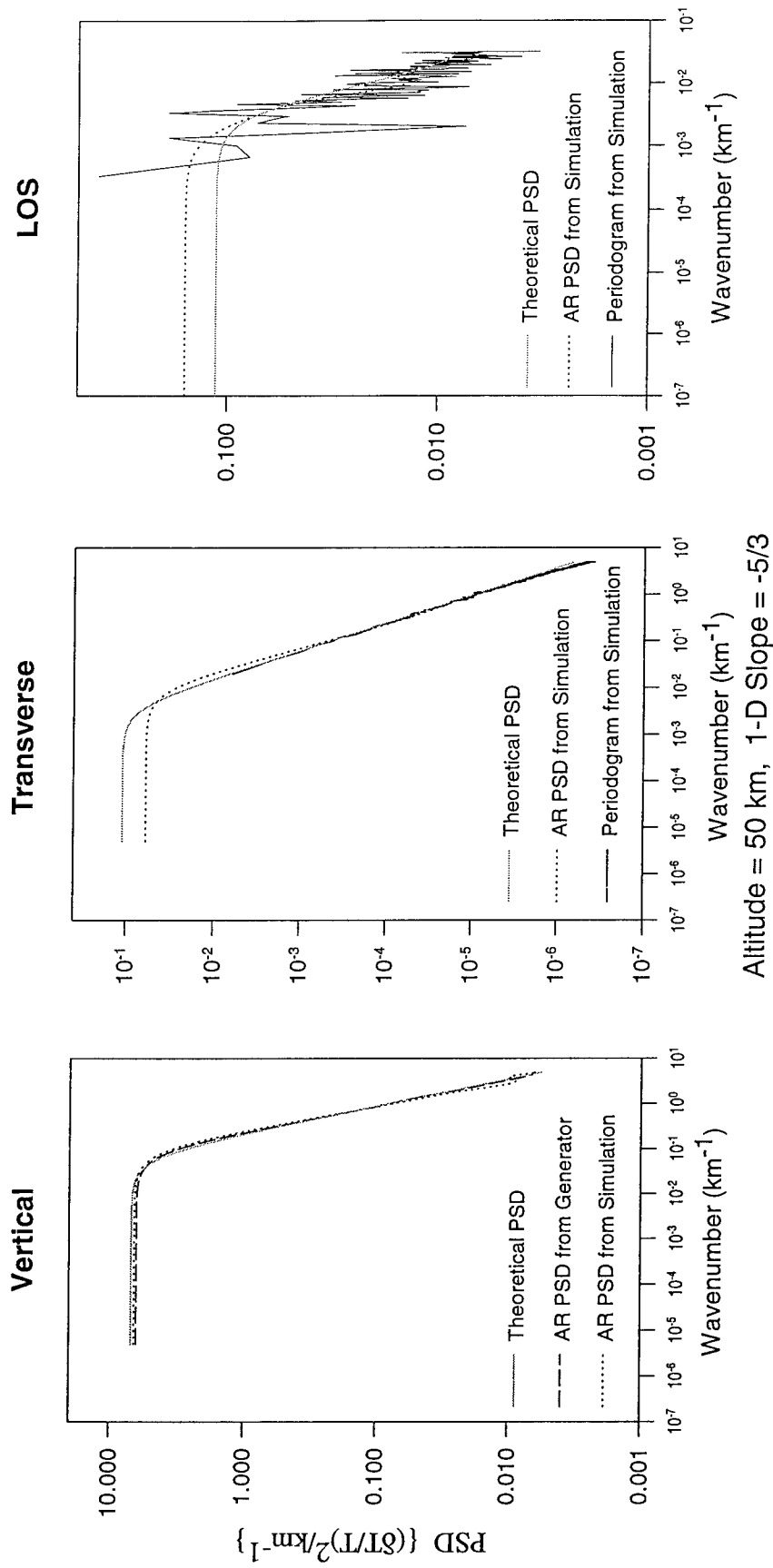


Figure 6. Graphs of Vertical, Transverse, and Line-of-sight One-dimensional Power Spectral Densities Plotted Against Spatial Frequency. The left panel plots the vertical PSDs for the theoretical model (light gray solid curve), autoregressive "generator" model (dashed curve), and the autoregressive vertical PSD from the simulated database (dotted curve). The middle panel plots the transverse PSDs for the theoretical model (light gray solid curve), autoregressive PSD from the simulated database (dotted curve), and a periodogram from the simulated database (solid curve). The right panel plots the line-of-sight PSDs for the theoretical model (light gray solid curve), autoregressive PSD from the simulated database (dotted curve), and a periodogram from the simulated database (solid curve). The plots are for 50.6 km altitude and one-dimensional high frequency spectral slope (S) = -5/3, where $\sigma^2 = 8.34 \times 10^{-4}$, $L_{cv} = 1.72$ km, $L_{ch} = 32.9$ km. The vertical spatial spacing = 0.1 km, transverse spacing = 0.1 km, and line-of-sight spacing = 15.7 km. The curves show log-log plots of PSDs measured in $\frac{(\delta T / \text{Temperature})^2}{\text{Wavenumber}}$ and wavenumber measured in km^{-1} . The vertical autoregressive PSD for the simulation was computed by calculating a 6-coefficient forward and backward autoregressive model of the vertically simulated data from layers extending from 50.0 km to 50.6 km in the forward direction and layers extending from 51.2 km to 50.6 km in the backward direction. Note that the "transverse" direction is defined as the horizontal perpendicular to the "line-of-sight" direction. The transverse and line-of-sight PSDs represent the 1-D component of the 2-D horizontal PSD having a high frequency horizontal spectral slope = -8/3. Their autoregressive PSDs result from computing a 10-coefficient autoregressive model of the transverse and line-of-sight simulated data in the layer at 50.6 km. The transverse Nyquist frequency is approximately $1/(2 \times 0.1) = 5 \text{ km}^{-1}$ and the line-of-sight Nyquist frequency is approximately $1/(2 \times 15.7) = 0.032 \text{ km}^{-1}$.

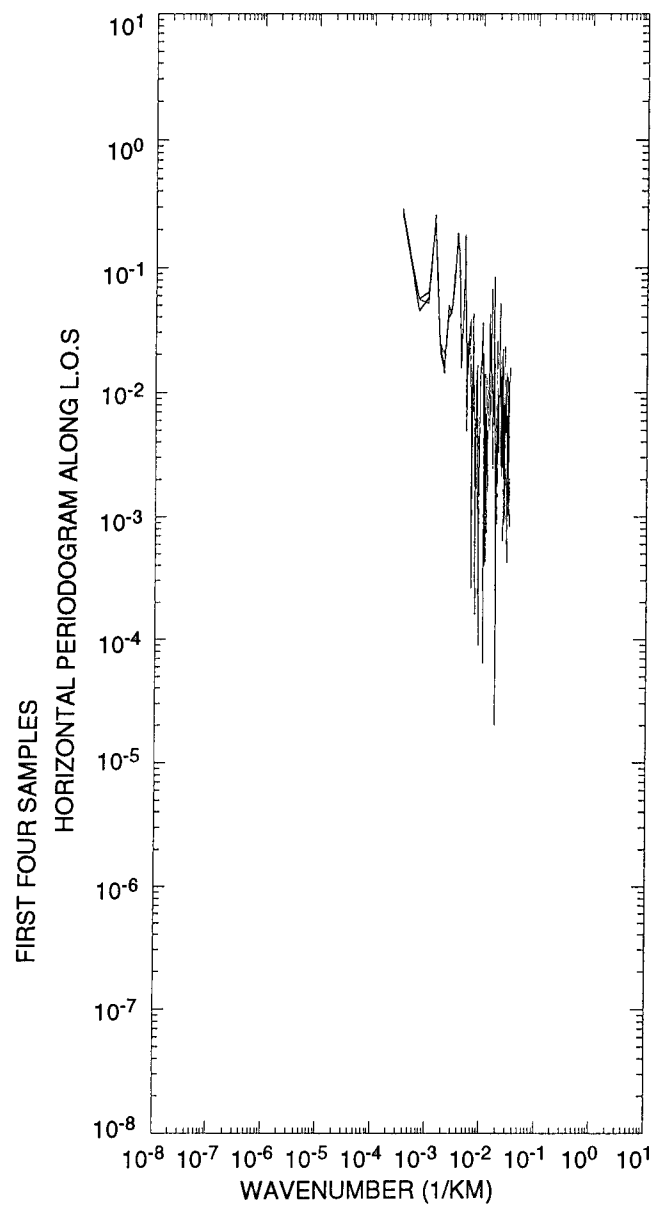


Figure 7. One-dimensional Periodograms of the First Four Samples of the Line-of-sight Simulated Data in the Layer at 50.6 km.

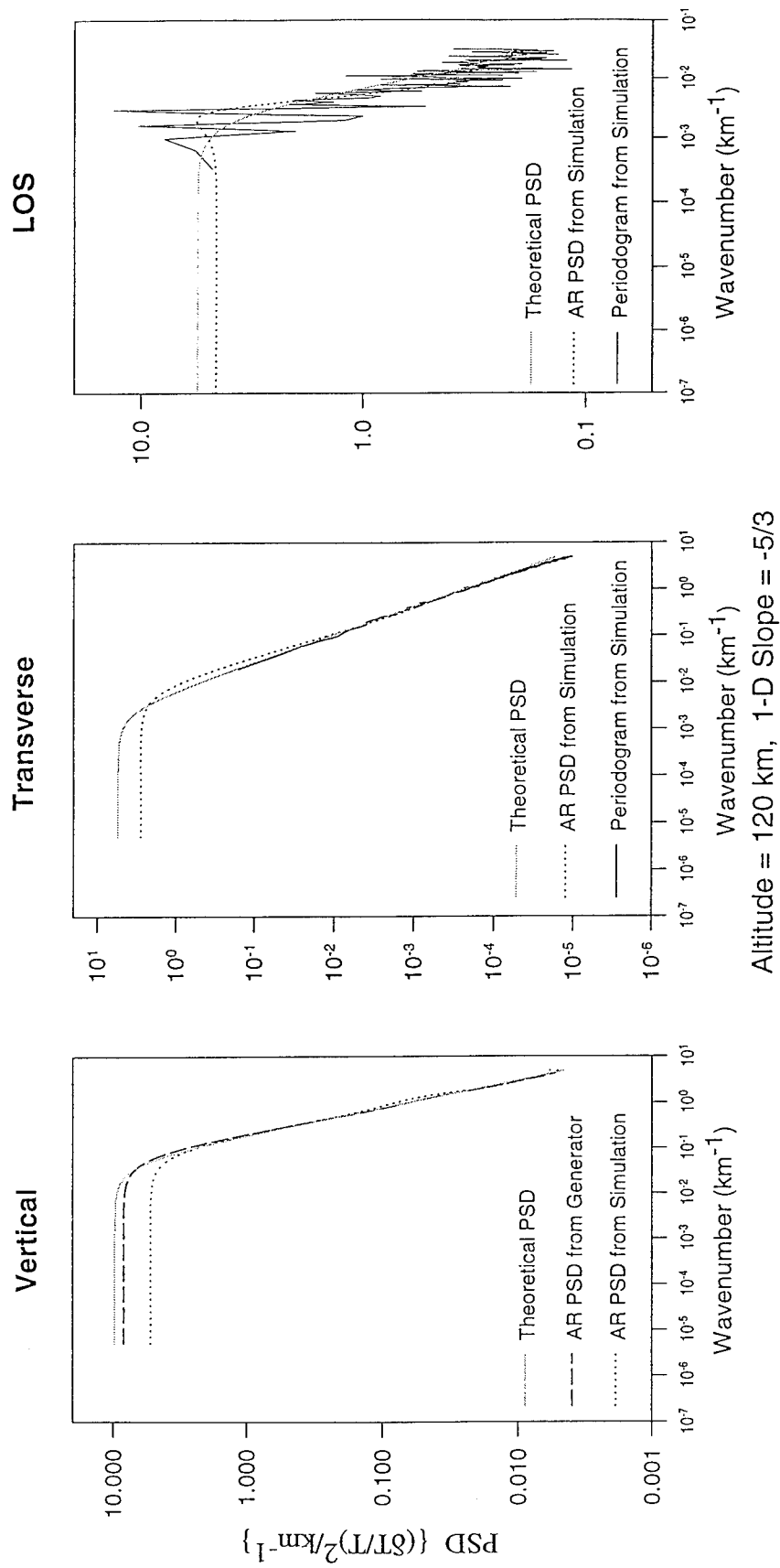


Figure 8. Same as Figure 6 Except Altitude = 119.3 km, $\sigma^2 = 0.0277$, $L_{cv} = 2.42$ km, $L_{ch} = 49.1$ km. The transverse spacing is 0.101 km and LOS spacing is 15.9 km.

Estimates of the correlation lengths and variances for the individual specifications and realizations presented in this report are shown in Table 2. Also, Table 3 provides the estimated error from the specified parameter values. The vertical database correlation length estimates are derived from the 6-coefficient forward and backward estimates of the vertical *PSD* while the horizontal database correlation length estimates are derived from the 10-coefficient estimates of the horizontal *PSD* along the line-of-sight direction. The estimated database variances are the actual variances computed from the database values themselves for the specified layer. Examination of Tables 2 and 3 tends to indicate that the error of an individual realization of correlation length falls within about 30 percent. Since the database represents a single sample from an ensemble of potential synthetic atmospheres (different random number seeds would yield additional samples), the estimated error seems reasonable. As the number of realizations expand it is expected that the estimate of the mean would converge to the specified values.

Table 2. Correlation Lengths: Specified vs Database Estimates

Database vs Specified Model Parameters							
		-5/3 slope			-3 slope		
		σ^2	L_{cv}	L_{ch}	σ^2	L_{cv}	L_{ch}
50 km	spec.	0.00083	1.72	32.9	0.00083	1.72	32.9
	dbase	0.00084	1.53	46.0	0.00082	2.17	30.1
89 km	spec.	0.0100	1.80	36.2	0.0100	1.80	36.2
	dbase	0.0092	1.76	33.1	0.0096	2.15	29.0
120 km	spec.	0.0277	2.42	49.1	0.0277	2.42	49.1
	dbase	0.0289	1.62	38.9	0.0289	2.21	35.2

Table 3. Estimated Errors, Specified Parameters vs Database Values

Percent Error, Database vs Specified Model Parameters						
	-5/3 slope			-3 slope		
	σ^2	L_{cv}	L_{ch}	σ^2	L_{cv}	L_{ch}
50 km	1	-11	39	-1	26	-9
89 km	-8	-2	-9	-4	19	-20
120 km	4	-33	-21	4	-9	-28

Figure 9 depicts the probability distribution histogram of the simulated data in the horizontal layer at 50.6 km, while Figure 10 depicts the cumulative distribution function. Visual comparison of the histogram with the theoretical (solid) curves indicate that the simulated data retains the Gaussian shape and that the standard deviation of the data falls within 8 percent of the theoretical value.

8. DATABASE

A random access data file consisting of 68,911,104 data points (701 vertical by 512 horizontal transverse by 192 LOS) was constructed. Each point was saved as an 8 bit byte, encoded between a minimum value of -128 and a maximum value of +127. A small separate corollary ASCII file was also saved that provided specification information about the random access file. The ASCII file also contained sets of linear transformation constants for each altitude. These constants allowed efficient computation of the relative temperature fluctuations from the byte data as $\frac{\delta T}{T} = c_1 + c_2 \times ByteValue$. A sample of the ASCII file is shown in Figure 11.

FILE POHMOD7 7-FEB-94 NUMBER OF CYCLES USED (ALIASING) L.O.S.=157 NUMBER OF CYCLES USED (ALIASING) PER L.O.S.=1
 MODIFY ZERO FREQ TO GIVE CORRECT VARIANCE GREAT CIRCLE APPROXIMATION EARTH RADIUS = 6370E+03
 RANDOM NUMBER SEED = 12345 ALTITUDE NUMBER 7 = 5.060E+01 SLOPE (V) = 1.67E+00 THIS MEANS NU(V) = 3.33E-01 SPACING(V) = 1.00E-01
 AV=6.90E-02 LCV=1.72E+00 NUMBER OF HORIZONTAL SAMPLES=98304 NUMBER OF PREDICTOR COEFFICIENTS V=6 H=10
 NUMBER OF ITERATIONS=51 THIS IS ONE SHEET OF 512 PERPENDICULAR VALUES BY 192 L.O.S. VALUES SIGMA**2 WILL BE SET TO 8.34E-04
 PERPENDICULAR SPACING=1.00E-01 SPACING L.O.S.=1.57E+01 AH=3.62E-03 LCH=3.29E+01 SLOPE(H)=2.67E+00 THIS MEANS NU(H)=3.33E-01

SOLID=THEORETICAL
 BARS=ACTUAL
 NUMBER OF POINTS=98304
 WEIGHTED AVERAGE SUBTRACTED
 -3.84E-03
 STANDARD DEVIATION OF DATA
 2.89E-02

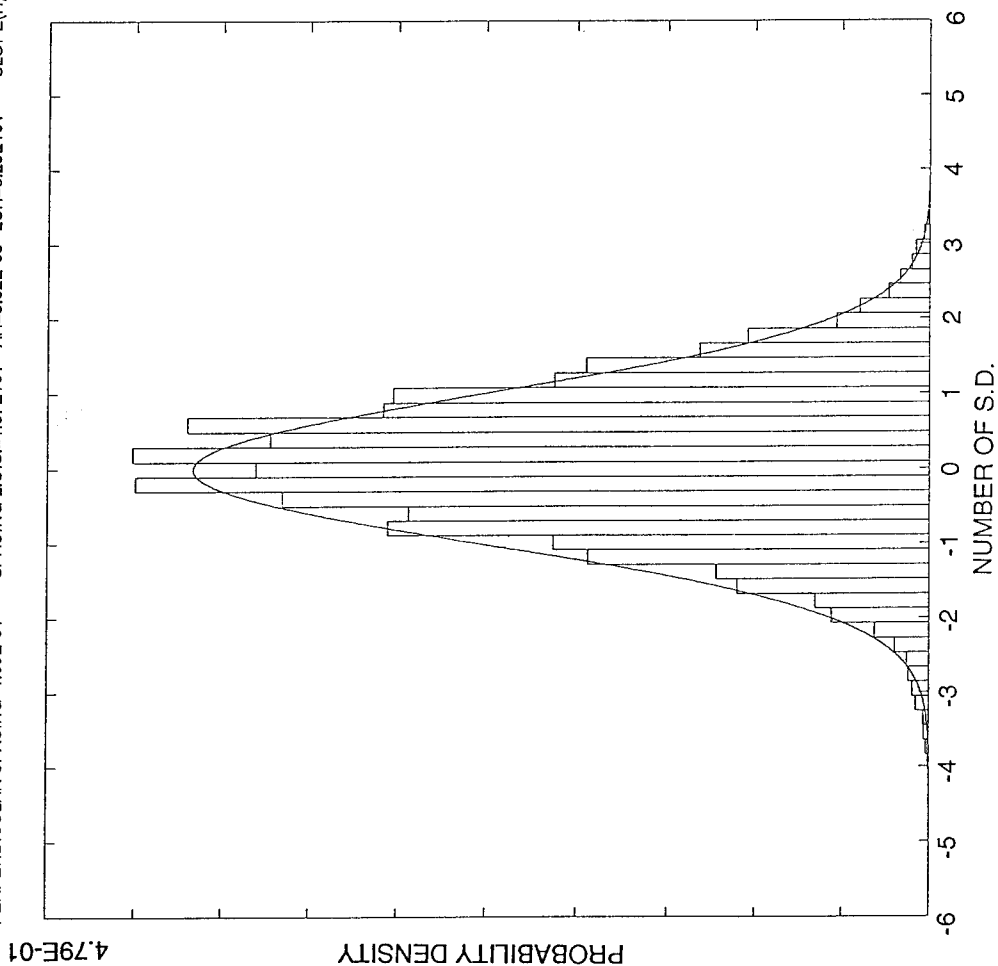


Figure 9. Histogram Representing the Probability Distribution Function of the Simulated Data at 50.6 km. Solid line is the theoretical Gaussian pdf. The variance of the data is 8.35×10^{-4} .

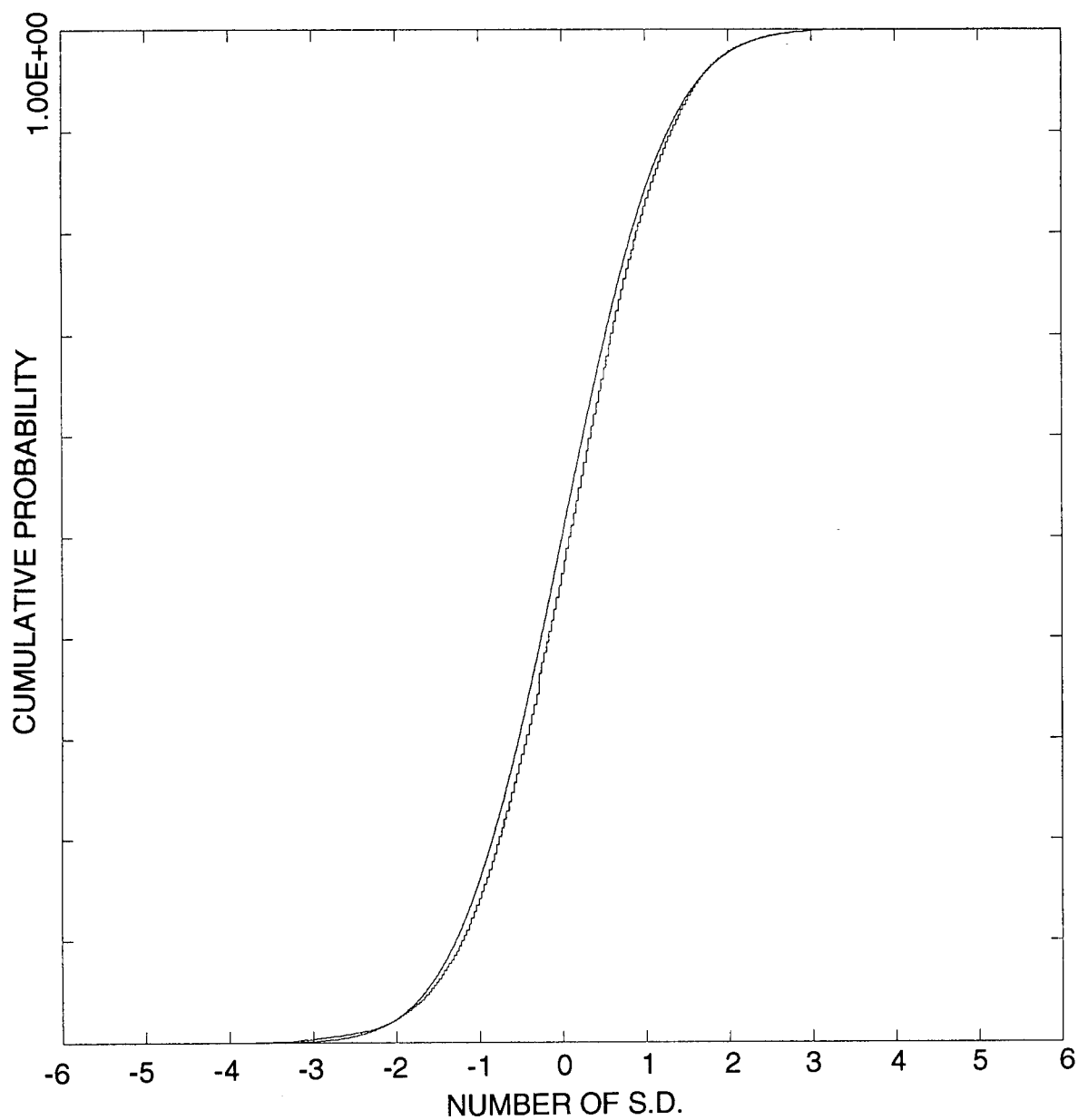


Figure 10. Cumulative Distribution Function of the Simulated Data at 50.6 km Compared to the Theoretical Curve.

```

12345 =RANDOM NUMBER SEED
7-FEB-94 OUTPUT FROM PROGRAM SCHMOD5
5.0000E+01 THIS IS Z1 LOWEST ALTITUDE SIMULATED
6.3700E+03 THIS IS RE THE RADIUS OF THE EARTH
TO CALCULATE THE TRANSVERSE DISTANCE DT AT ALTITUDE Z
FOR POINT NUMBER NPT,WITH SPACING AT Z1 OF DX
(DIFFERENT ALONG THE LINE OF SIGHT AND PERPENDICULAR
TO THE LINE OF SIGHT),
USE THE FORMULA DT=(RE+Z)*DX*(NPT-1)/(RE+Z1)
2.6667E+00 SLOPE OF PSD HORIZONTAL (2-D)
1.6667E+00 SLOPE OF PSD VERTICAL (1-D)
1.0000E-01 SPACING (KM) HORIZONTAL RESULT PERPENDICULAR L.O.S. LOWEST ALTITUDE
1.0000E-01 SPACING (KM) VERTICAL RESULT
512 NUMBER OF VALUES PERPENDICULAR LINE OF SIGHT
701 NUMBER OF VERTICAL VALUES
192 NUMBER OF VALUES ALONG LINE OF SIGHT
51 NUMBER OF SHEETS FOR INITIALIZATION
1.5707E+01 SPACING (KM) ALONG LINE OF SIGHT
157 NUMBER OF CYCLES FOR ALIASING L.O.S
1 NUMBER OF CYCLES FOR ALIASING PERPENDICULAR L.O.S
-5.7000E-01 =PSD BIAS
CREATE A FILE CONSISTING OF BYTES
EACH OF WHICH REPRESENTS A NUMBER BETWEEN -128 AND +127.
THIS IS DIVIDED INTO RECORDS AS THE FOLLOWING LOGIC INDICATES
NUM=0
DO I=1,NUMBER OF ALTITUDES
DO J=1,NUMBER OF POINTS ALONG TO THE LINE OF SIGHT
NUM=NUM+1
WRITE (8,REC=NUM) (VALUE(I,K,J),K=1,NUMBER OF POINTS PERPENDICULAR L.O.S.)
END DO
END DO
FOR I= 1,ALTITUDE= 5.0000E+01KM, (DT/T)= -2.8273E-03+ 7.8602E-04*VALUE
FOR I= 2,ALTITUDE= 5.0100E+01KM, (DT/T)= -9.5905E-03+ 7.8048E-04*VALUE
FOR I= 3,ALTITUDE= 5.0200E+01KM, (DT/T)= -1.1463E-02+ 7.8550E-04*VALUE
FOR I= 4,ALTITUDE= 5.0300E+01KM, (DT/T)= -1.2085E-02+ 7.1519E-04*VALUE
FOR I= 5,ALTITUDE= 5.0400E+01KM, (DT/T)= -9.6289E-03+ 7.2735E-04*VALUE
FOR I= 6,ALTITUDE= 5.0500E+01KM, (DT/T)= -1.5482E-02+ 8.2105E-04*VALUE
FOR I= 7,ALTITUDE= 5.0600E+01KM, (DT/T)= -1.1941E-02+ 8.7036E-04*VALUE
FOR I= 8,ALTITUDE= 5.0700E+01KM, (DT/T)= -1.5864E-02+ 8.8468E-04*VALUE
FOR I= 9,ALTITUDE= 5.0800E+01KM, (DT/T)= -1.2681E-02+ 9.0684E-04*VALUE
FOR I= 10,ALTITUDE= 5.0900E+01KM, (DT/T)= -8.8909E-03+ 9.6629E-04*VALUE
FOR I= 11,ALTITUDE= 5.1000E+01KM, (DT/T)= -6.6515E-03+ 8.9558E-04*VALUE
FOR I= 12,ALTITUDE= 5.1100E+01KM, (DT/T)= 3.0155E-03+ 9.3763E-04*VALUE
FOR I= 13,ALTITUDE= 5.1200E+01KM, (DT/T)= 1.3740E-04+ 8.5331E-04*VALUE
FOR I= 14,ALTITUDE= 5.1300E+01KM, (DT/T)= -1.4131E-03+ 7.9499E-04*VALUE
FOR I= 15,ALTITUDE= 5.1400E+01KM, (DT/T)= -9.1715E-03+ 8.3941E-04*VALUE
FOR I= 16,ALTITUDE= 5.1500E+01KM, (DT/T)= -8.3961E-03+ 9.5934E-04*VALUE
FOR I= 17,ALTITUDE= 5.1600E+01KM, (DT/T)= -1.4722E-03+ 8.8723E-04*VALUE
FOR I= 18,ALTITUDE= 5.1700E+01KM, (DT/T)= -4.9128E-03+ 8.2328E-04*VALUE
FOR I= 19,ALTITUDE= 5.1800E+01KM, (DT/T)= -4.3047E-03+ 8.3197E-04*VALUE
FOR I= 20,ALTITUDE= 5.1900E+01KM, (DT/T)= -6.3201E-03+ 7.6369E-04*VALUE
FOR I= 21,ALTITUDE= 5.2000E+01KM, (DT/T)= 2.5905E-03+ 7.7723E-04*VALUE
FOR I= 22,ALTITUDE= 5.2100E+01KM, (DT/T)= -4.8177E-03+ 8.6719E-04*VALUE
FOR I= 23,ALTITUDE= 5.2200E+01KM, (DT/T)= -2.3910E-03+ 9.4519E-04*VALUE
FOR I= 24,ALTITUDE= 5.2300E+01KM, (DT/T)= -1.0030E-02+ 8.6416E-04*VALUE
FOR I= 25,ALTITUDE= 5.2400E+01KM, (DT/T)= -1.4973E-02+ 9.4909E-04*VALUE
FOR I= 26,ALTITUDE= 5.2500E+01KM, (DT/T)= 5.9302E-04+ 8.4785E-04*VALUE
FOR I= 27,ALTITUDE= 5.2600E+01KM, (DT/T)= -4.3746E-03+ 8.0043E-04*VALUE
FOR I= 28,ALTITUDE= 5.2700E+01KM, (DT/T)= -1.9294E-03+ 8.1456E-04*VALUE
FOR I= 29,ALTITUDE= 5.2800E+01KM, (DT/T)= -4.9838E-03+ 8.1147E-04*VALUE

```

Figure 11. Sample Page From the Database Explanation File.

9. SYNTHETIC 2-D SCENE FOR AN IMAGINARY TEMPERATURE SENSOR

The availability of a three-dimensional temperature structure database allows us to perform computer simulations of particular sensors viewing such an atmospheric environment. This ability enables us to perform economical tests and experimentation of more fundamental processes. To demonstrate the utility of the database, we will examine the effects of viewing the simulated atmosphere from an imaginary temperature sensor platform located at an altitude of 85 km. We will use a database generated with a $-5/3$ power spectral density power law. For these purposes, we imagine that our chosen sensor has the ability to integrate temperature fluctuations along its line-of-sight. Our computerized arbitrary sensor is an array of 512 horizontal pixels by 350 vertical pixels. The sensor viewing geometry is a rectangular cone having a full horizontal included angle of 2.19° and a full vertical included angle of 1.48° . Thus each pixel "looks" along its own line-of-sight and "sees" 0.0042° in both the horizontal and vertical direction. The sensor plane is tilted downward with the center pixel having a zenith angle of 95.23° . This geometry prescribes that the center pixel in the bottom row "looks" along a ray that has a tangent altitude of 50 km. Since we wish to "view" as much of the simulated atmosphere as possible, the forward distance at 85.2 km altitude (away from the sensor) is specified to have an arc length of 1,343 km. At this distance, the vertically viewed plane perpendicular to the line-of-sight has a horizontal and vertical spatial resolution of 0.1 km. The geometry is shown in Figure 12.

The integrated temperature structure along selected pixel rows in zenith look angles from the minimum of 94.6° to the maximum of 96° is depicted in Figure 13. The figure shows computations of $\int \{\Delta t(z)\} dz$ as plotted against the full range of horizontal look angles across the sensor. Here $\Delta t(z)$ are the temperature fluctuations along a particular line-of-sight z . Figure 14 shows similar plots but this time the temperature structure along selected pixel columns comprising horizontal look angles from -1.07° to $+1.07^\circ$ is plotted against the full range of zenith look angles. Taken together, the plots provide a two-dimensional spatial visualization of the integrated horizontal and vertical structure as "detected" by our imaginary temperature sensor. These spatial series may be analyzed by Fourier Transform analysis and, separately, by autoregressive analysis to provide estimates of the power spectral densities of the integrated structure as detected by the sensor. Figure 15 depicts 10 Fourier periodograms of the horizontally scanned simulated atmosphere for the same 10 zenith angles as Figure 13. Figure 16 uses 6-coefficient autoregressive analysis to provide the PSD estimates. Examination of these plots indicate that the power spectral density slope was transformed from the $-5/3$ database slope to an image plane slope of -2 . This is a surprising and not well understood result, which may be important in analyzing atmospheric radiance measurements or when simulating radiance structure from correlation overlay maps. Additional two-dimensional temperature structure scenes were computed using the -3 database spectral slope. Results showed that the larger slope was not transformed; instead, the image plane slope retained the -3 value. Investigations are continuing to identify the processes leading to these results.

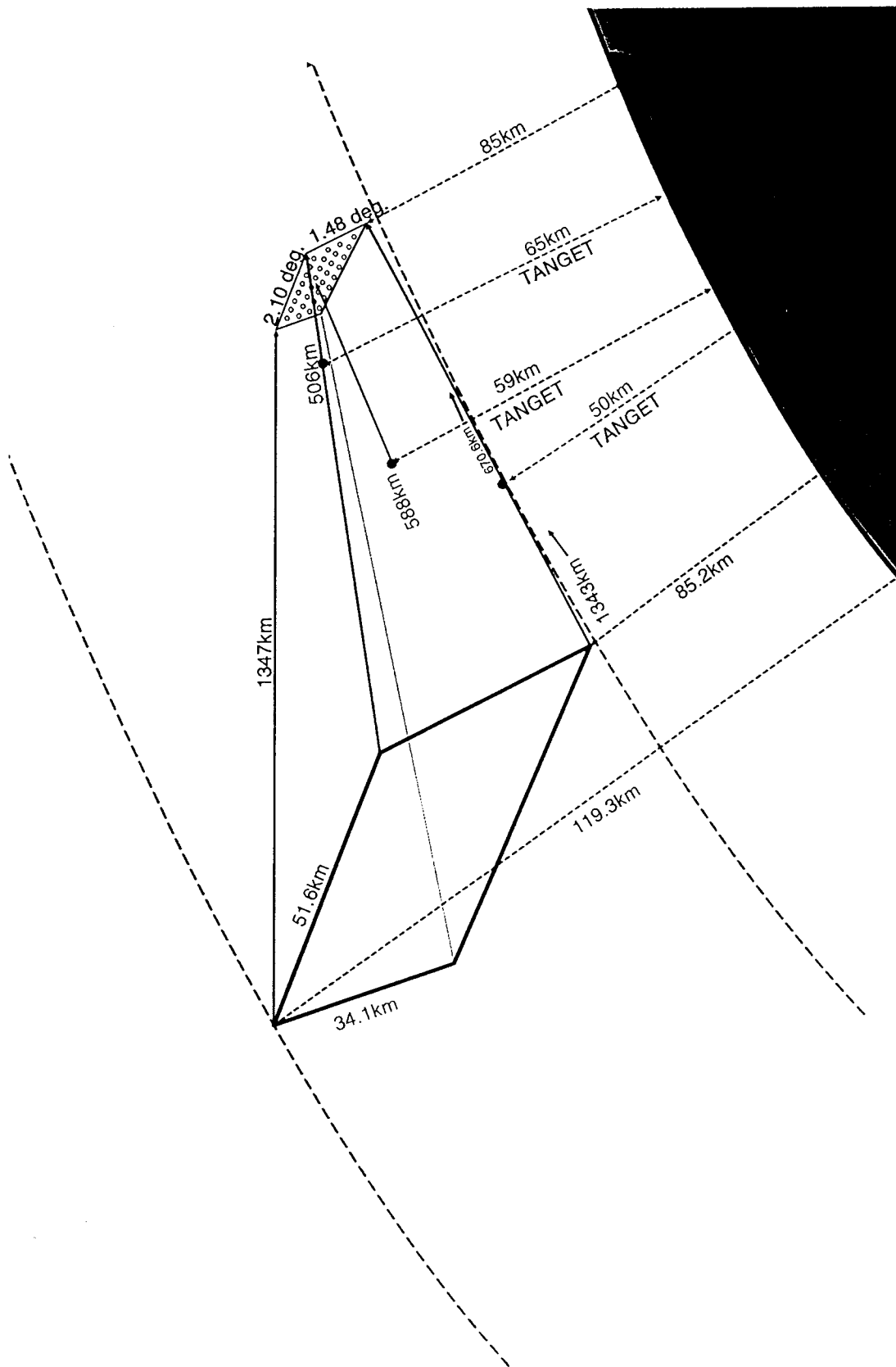


Figure 12. Viewing Geometry of an Imaginary Temperature Sensor Platform Located at an altitude of 85 km.

ALTITUDE OF OBSERVER= 8.50E+01 LOWEST ALTITUDE SIMULATED = 5.00E+01 2-D SLOPE OF PSD HORIZONTAL = 2.67E+00
 1-D SLOPE OF PSD VERTICAL= 1.67E+00 TRANSVERSE SPACING AT LOWEST ALTITUDE= 1.00E-01 VERTICAL SPACING= 1.00E-01
 SPACING ALONG L.O.S. = 1.57E+01 NUMBER TRANSVERSE POINTS = 512 NUMBER L.O.S. POINTS=192 NUMBER OF VERTICAL SHEETS = 701
 MAXIMUM ANGLE L.O.S. USED = 1.19E+01 DEGREES NUMBER OF ZENITH VALUES CALCULATED=350 CENTER ZENITH VALUE= 9.52E+01 DEGREES
 ZENITH SPACING= 4.20E-03 DEGREES NUMBER OF ALPHA VALUES CALCULATED=512 ALPHA SPACING= 4.20E-03

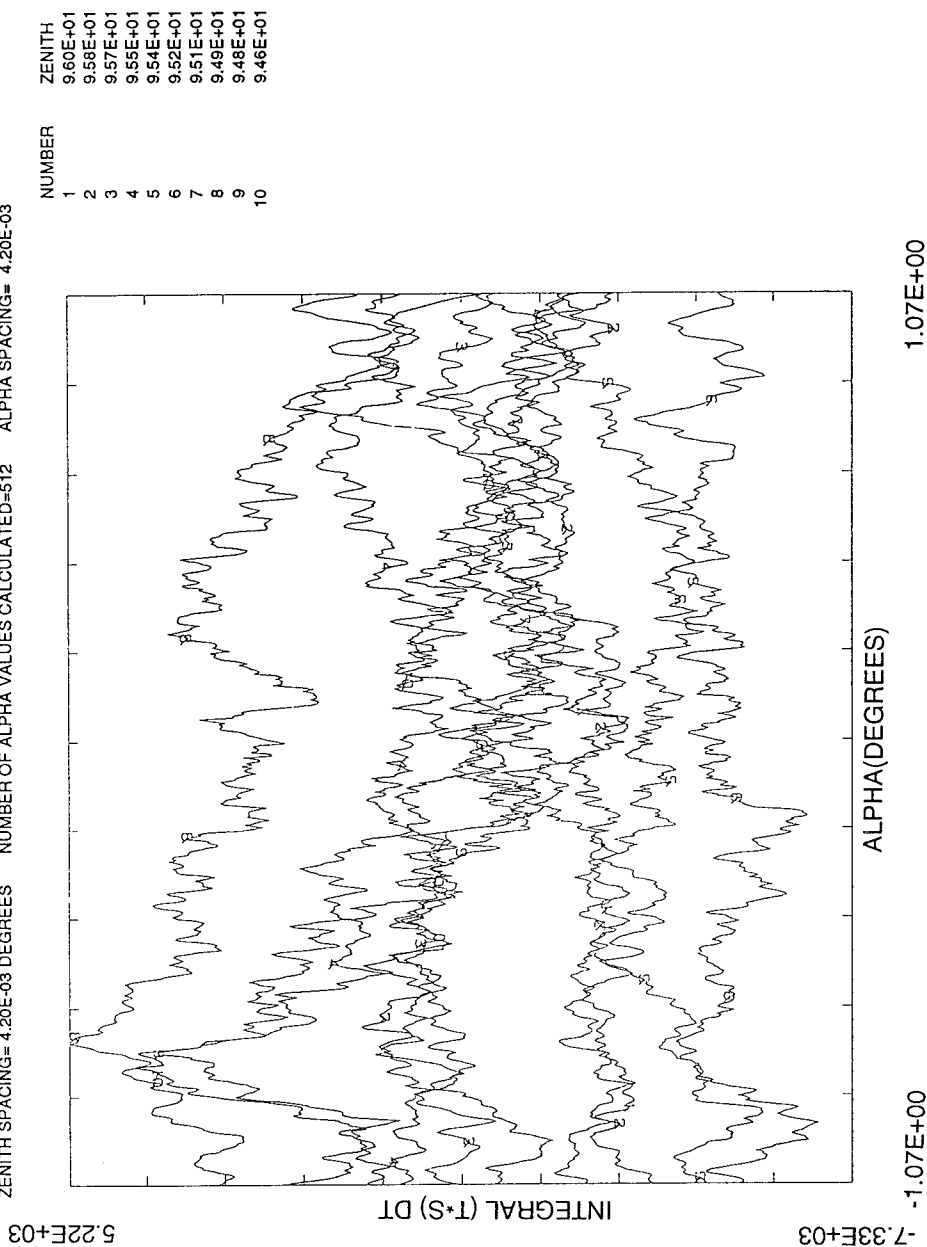


Figure 13. Integrated Temperature Structure Along Selected Pixel Rows Comprising Zenith Look
 Angles From the Minimum of 94.6° to the Maximum of 96°.

ALTITUDE OF OBSERVER= 8.50E+01 LOWEST ALTITUDE SIMULATED = 5.00E+01 2-D SLOPE OF PSD HORIZONTAL = 2.67E +00
 1-D SLOPE OF PSD VERTICAL= 1.67E+00 TRANSVERSE SPACING AT LOWEST ALTITUDE= 1.00E-01 VERTICAL SPACING= 1.00E-01
 SPACING ALONG L.O.S. = 1.57E+01 NUMBER TRANSVERSE POINTS = 512 NUMBER L.O.S. POINTS=192 NUMBER OF VERTICAL SHEETS = 701
 MAXIMUM ANGLE L.O.S. USED = 1.19E+01 DEGREES NUMBER OF ZENITH VALUES CALCULATED=350 CENTER ZENITH VALUE= 9.52E+01 DEGREES
 ZENITH SPACING= 4.20E-03 DEGREES NUMBER OF ALPHA VALUES CALCULATED=512 ALPHA SPACING= 4.20E-03

NUMBER	ALPHA
1	-1.07E+00
2	-8.59E-01
3	-6.45E-01
4	-4.31E-01
5	-2.16E-01
6	-2.10E-03
7	2.12E-01
8	4.26E-01
9	6.40E-01
10	8.55E-01
11	1.07E+00

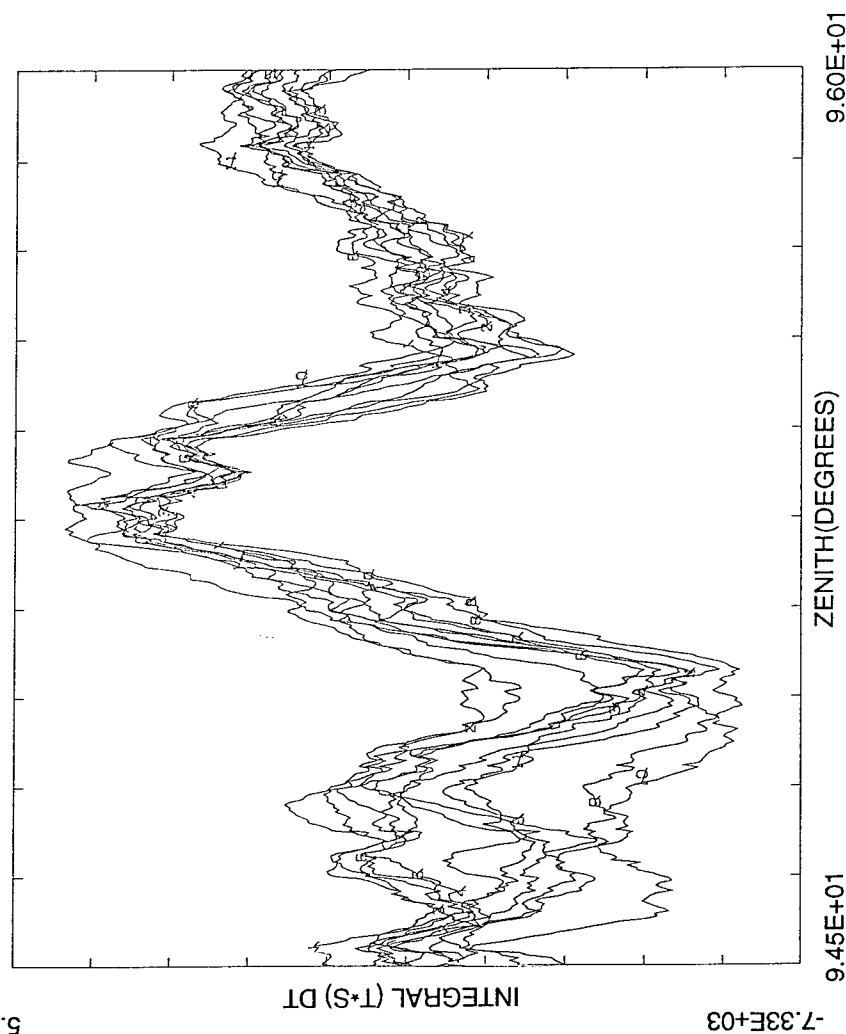


Figure 14. Integrated Temperature Structure Along Selected Pixel Columns Comprising Horizontal Look Angles From -1.07° to $+1.07^\circ$.

ALTITUDE OF OBSERVER = 8.50E+01 LOWEST ALTITUDE SIMULATED = 5.00E+01 2-D SLOPE OF PSD HORIZONTAL = 2.67E+00
 1-D SLOPE OF PSD VERTICAL = 1.67E+00 TRANSVERSE SPACING AT LOWEST ALTITUDE = 1.00E-01 VERTICAL SPACING = 1.00E-01
 SPACING ALONG L.O.S. = 1.57E+01 NUMBER TRANSVERSE POINTS = 512 NUMBER L.O.S. POINTS = 192 NUMBER OF VERTICAL SHEETS = 701
 MAXIMUM ANGLE L.O.S. USED = 1.19E+01 DEGREES NUMBER OF ZENITH VALUES CALCULATED = 350 CENTER ZENITH VALUE = 9.52E+01 DEGREES
 ZENITH SPACING = 4.20E-03 DEGREES NUMBER OF ALPHA VALUES CALCULATED = 512 ALPHA SPACING = 4.20E-03

NUMBER	ZENITH
1	9.60E+01
2	9.58E-01
3	9.57E-01
4	9.55E-01
5	9.54E-01
6	9.52E-01
7	9.51E-01
8	9.49E-01
9	9.48E-01
10	9.46E-01

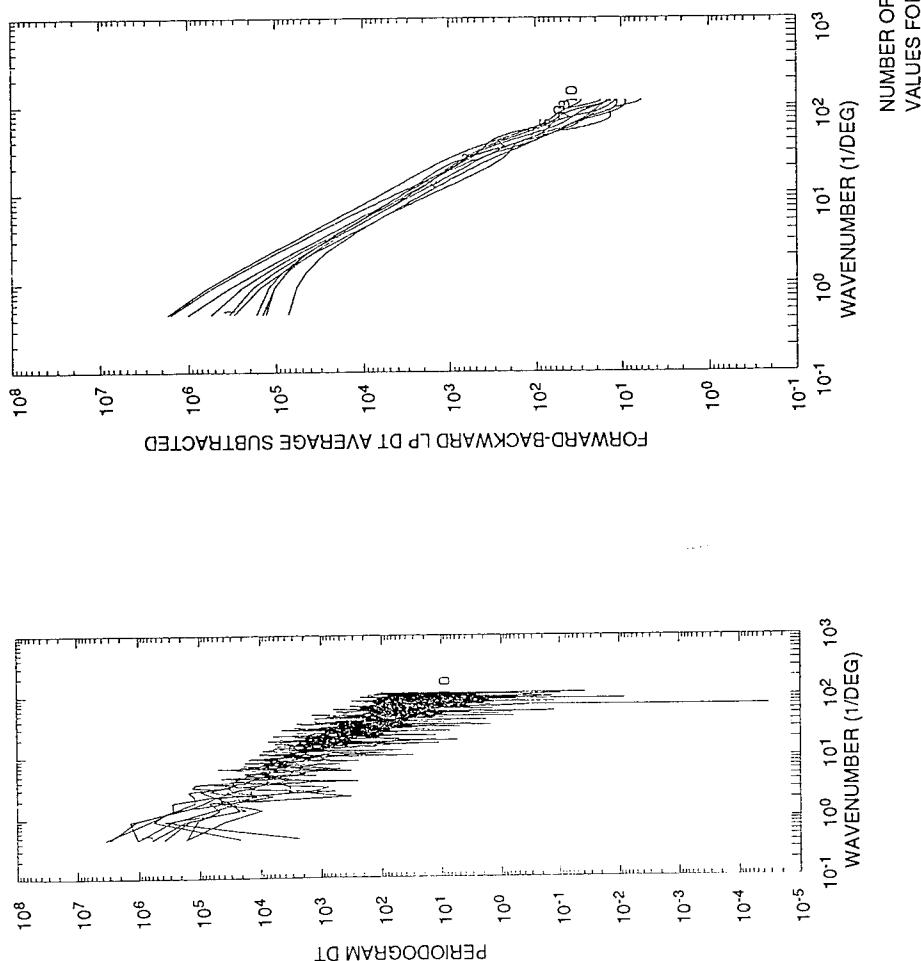


Figure 15. Fourier Periodograms of the Horizontally Scanned Simulated Atmosphere for the Same Look Angles as Figure 13.

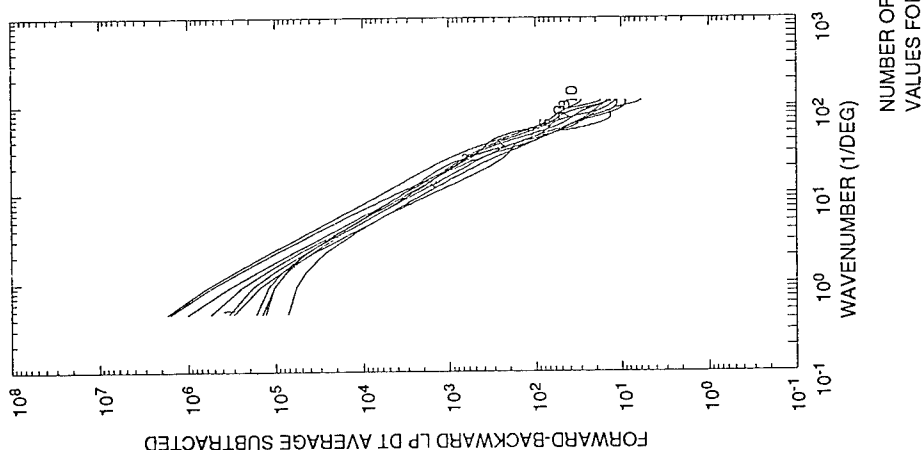


Figure 16. PSD Estimates of the Horizontally Scanned Simulated Atmosphere From Autoregressive Analysis.

The full two-dimensional integrated temperature structure "scene" is depicted in Figure 17. Clearly, the figure shows that the three-dimensional hybrid method provides matrix realizations having significant utility for computer sensor simulations. The technique preserves relatively large horizontal correlations and relatively small vertical correlations. As Figure 17 also shows, use of the matrix realizations leads to a better understanding of underlying processes and provides some unexpected results in the two-dimensional scene.

10. CONCLUSION

Geophysical phenomena within a specified domain often are characterized by smooth continuous power spectral densities having a negative power law slope. A stochastic one-dimensional autoregressive approach was employed to generate vertically correlated synthetic data, and two-dimensional fast Fourier transform synthesis was used to generate horizontally correlated data from the vertically structured arrays. The joint goals of reducing the computational burden and of generating three-dimensional non-stationary synthetic structure databases that are faithful to the theoretical descriptions were achieved. A complete random access database file consisting of 68,911,104 points was generated on the Phillips Laboratory model 210 Convex computer with an average execution time of 2.5 hrs. The process preserved the power spectral density law, correlation scale, variance, and probability density function. A 6-coefficient autoregression model accurately simulated the 701 point vertical structure and a 512 x 192 point 2-D FFT accurately provided the horizontal structure. The three-dimensional hybrid method provides matrix realizations having significant utility for computer sensor simulations. We have demonstrated the utility of the three-dimensional database and we examined the effects of viewing the simulated atmosphere from an imaginary temperature sensor platform located at an altitude of 85 km. Use of the matrix realizations leads to a better understanding of underlying processes and provides some unexpected results in the two-dimensional scene. We have shown that the integrated temperature structure preserves the relatively large horizontal correlations and relatively small vertical correlations but that the $-5/3$ power spectral density slope is transformed by the line-of-sight integration through several layers. This is a surprising and not well understood result which may be important in analyzing atmospheric radiance measurements or when simulating radiance structure from correlation overlay maps. In contrast, the -3 power spectral density slope was unaltered by the integration process. Studies are continuing with the hope of identifying the processes leading to these different results.

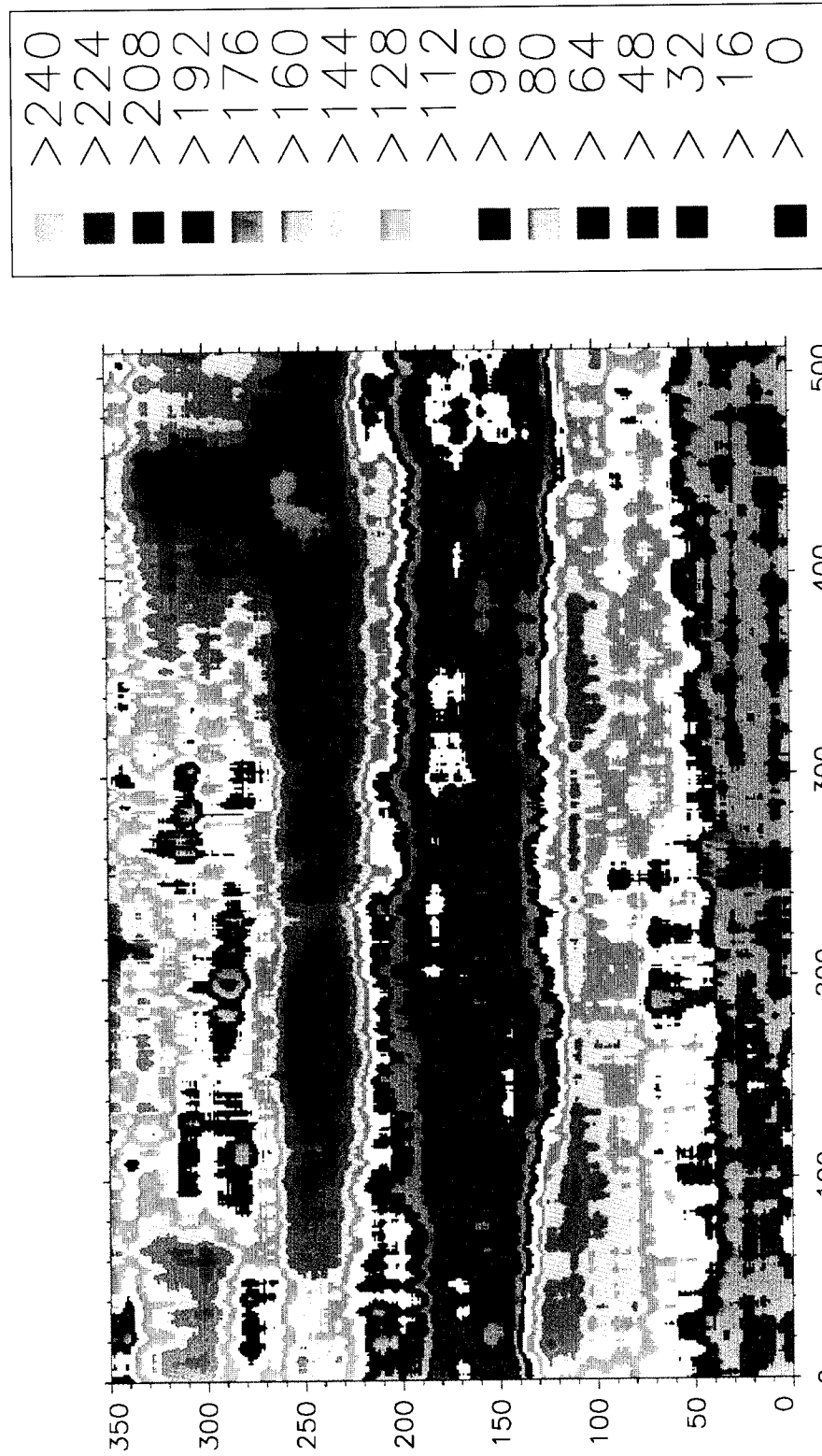


Figure 17. Full Two-dimensional Integrated Temperature Structure "Scene".

References

1. Sharma, R.D., Duff, J.W., Sundberg, R.L., Gruninger, J.H., Bernstein, L.S., Robertson, D.C., and Healey, R.J. (1991) *Description of SHARC-2, The Strategic High Altitude Atmospheric Radiance Code*, Phillips Laboratory Tech. Rpt., PL-TR-91-2071. ADA239008
2. Gruninger, J., Sundberg, R.L., Duff, J.W., Bernstein, L.S., Matthew, M.W., Adler-Golden, S., Robertson, D., Sharma, R., Brown, J.H., Healey, R., and Vail J. (1994) SHARC - 3, A Model for Infrared Radiance at High Altitudes, *Proc. SPIE - The International Society of Optical Engineering*, V:2223, Orlando, Florida.
3. Sundberg, R.L., Gruninger, J., De, P., and Brown, J.H. (1994) Infrared radiance fluctuations in the upper atmosphere, *Proc. SPIE - The International Society of Optical Engineering*, V:2223, Orlando, Florida.
4. Sears, R.D., Strugala, L.A., Newt, J., Robertson, D., Brown, J.H., and Sharma, R. (1994) Simulation of the Infrared Structured Earthlimb Background Using the SHARC Radiance Code, *32nd Aerospace Sciences Meeting and Exhibit*, Reno, NV.
5. Brown, J.H. (1993) *Atmospheric Structure Simulation: An Autoregressive Model for Smooth Geophysical Power Spectra with Known Autocorrelation Function*, Phillips Laboratory Tech. Rpt., PL-TR-93-2185, ERP No. 1128, ADA 276691.
6. Brown, J.H. (1993) *Atmospheric Structure Simulation: An ARMA Model for Smooth Isotropic Two-Dimensional Geophysical Power Spectra*, Phillips Laboratory Tech. Rpt., PL-TR-93-2224, ERP No. 1132, ADA 280476.
7. Marple, S.L. (1987) *Digital Spectral Analysis with Applications*, Chapter 6, Prentice-Hall, Englewood, New Jersey.
8. Kay, Steven M. (1988) *Modern Spectral Estimation, Theory & Application*, Prentice-Hall, Englewood, New Jersey.
9. Tatarski, V.I. (1961) *Wave Propagation in a Turbulent Medium*, McGraw-Hill.

10. Futterman, W.I., Schweitzer, E.L., and Newt, J.E. (1991) Estimation of scene correlation lengths, characterization, propagation, and simulation of sources and backgrounds, *Proc. SPIE - The International Society of Optical Engineering*, **V**:1486, pp127-140, Orlando, Florida.
11. For the integral, see for example, Gradshteyn, I.S. and Ryzhik, I.M. (1965) *Table of Integrals Series and Products*, eq 3.241.4, Academic Press.
12. Gradshteyn, I.S. and Ryzhik, I.M. (1965) *Table of Integrals Series and Products*, eq 8.432.5, Academic Press.
13. Bracewell, R.N. (1978) *The Fourier Transform and Its Applications*, McGraw-Hill, New York.
14. Strugala, L.A., (1991) Development of high resolution statistically non-stationary infrared earthlimb radiance scenes, characterization, propagation, and simulation of sources and backgrounds, *Proc. SPIE - The International Society for Optical Engineering*, **V**:1486, pp. 176-187, Orlando, Florida.
15. Strugala, L.A. (1993) Production of statistically nonstationary stochastic structure realizations for infrared background scene simulations, *Optical Engineering*, **V32**(No5):, pp. 993-1001.
16. Haykin, Simon, ed. (1991) *Advances in Spectrum Analysis and Array Processing*, V1, Prentice Hall, Englewood Cliffs, New Jersey, pp.155-156.

Appendix

Computational Details

A1. LINE-OF-SIGHT PSD TRUNCATION CORRECTION

Since the constructed database has a finite and relatively large line-of-sight data spacing, a natural truncation of the line-of-sight power spectral density function must occur that would cause significant aliasing of the line-of-sight PSDs for any particular realization. The database has a horizontal transverse Nyquist frequency (k_{NY_t}) of about 5 km^{-1} , and a line-of-sight Nyquist frequency (k_{NY_ℓ}) of about 0.032 km^{-1} . Our treatment assumes the $PSD = 0$ beyond k_{NY_t} . Since significant energy exists between (k_{NY_ℓ}) and k_{NY_t} , aliasing must occur in the LOS direction. Consequently, computational "aliasing" of the line-of-sight PSDs was added to the "theoretical" PSDs by the following formulation. For an isotropic two-dimensional power density spectrum having frequencies k_t and k_ℓ , with Nyquist frequencies k_{NY_t} and (k_{NY_ℓ}), the estimated power spectral density (PSD_e) is:

$$PSD_e(k_t, k_\ell) = PSD(k_t, k_\ell) + PSD(k_t, 2k_{NY_\ell} - k_\ell) + PSD(k_t, 2k_{NY_\ell} + k_\ell)$$

$$+ PSD(k_t, 4k_{NY_\ell} - k_\ell) + PSD(k_t, 4k_{NY_\ell} + k_\ell) + \dots$$

until the second argument becomes greater than k_{NY_t} . Each term in the series on the right forms an aliasing branch as depicted in Figure A1. Two special cases apply.

At $k_\ell = 0$, $PSD_e(k_t, 0) = PSD(k_t, 0) + PSD(k_t, 2k_{NY_\ell}) + PSD(k_t, 4k_{NY_\ell}) + \dots$.

Also, at $k_\ell = k_{NY_\ell}$, $PSD_e(k_t, k_{NY_\ell}) = PSD(k_t, 2k_{NY_\ell}) + PSD(k_t, 3k_{NY_\ell}) + PSD(k_t, 5k_{NY_\ell}) + \dots$.

Hence, the computation of $PSD_e(k_t, k_\ell)$ was the "theoretical" horizontal PSD that was used in construction of the simulated database. The above applies since the two-dimensional discrete Fourier Transform, $F(k_t, k_\ell)$, of a function $f(t, \ell)$ is:

$$F(k_t, k_\ell) = \sum_{j=0}^{N_t} \sum_{l=0}^{N_\ell} f(t_j, \ell_l) e^{-itk_t} e^{-i\ell k_\ell} \quad \text{for } 0 \leq k_t, k_\ell \leq \pi,$$

and since,

$$e^{-i\ell(2\pi - k_\ell)} = e^{-i\ell k_\ell} = \left(e^{-i\ell k_\ell}\right)^* \quad \text{and} \quad e^{-i\ell(2\pi + k_\ell)} = e^{-i\ell k_\ell} = \left(e^{-i\ell k_\ell}\right)^*.$$

This implies that the $PSD(k_t, 2\pi - k_\ell)$ contributes to the PSD of $f(t, \ell)$ at frequency k_t, k_ℓ and the $PSD(k_t, 2\pi + k_\ell)$ also contributes to the PSD of $f(t, \ell)$.

FILE PCHMOD6 7-FEB-94 GREAT CIRCLE APPROXIMATION EARTH RADIUS = 6.370E+03
 NUMBER OF CYCLES USED (ALIASING) L.O.S. = 15Z NUMBER OF CYCLES USED (ALIASING) PER L.O.S. = 1
 RANDOM NUMBER SEED = 12345 ALTITUDE = 5.060E+01 SLOPE (V) = 1.67E+00 THIS MEANS NU(V) = 3.33E-01 SPACING(V) = 1.00E-01
 AV = 6.90E-02 LCV = 1.72E+00 NUMBER OF HORIZONTAL SAMPLES = 98304 NUMBER OF PREDICTOR COEFFICIENTS V = 6 H = 6
 NUMBER OF ITERATIONS = 51 THIS IS ONE SHEET OF 512 PERPENDICULAR VALUES BY 1192 L.O.S. VALUES SIGMA+2 WILL BE SET TO 8.34E-04
 PERPENDICULAR SPACING = 1.00E-01 SPACING L.O.S. = 1.57E+01 AH = 3.62E-03 LCH = 3.29E+01 SLOPE(H) = 2.67E+00 THIS MEANS NU(H) = 3.33E-01
 INTEGRAL OF PSD = 8.23E-04
 THIS IS SHEET NUMBER 7
 BIAS PSD MODEL TO GIVE CORRECT VARIANCE

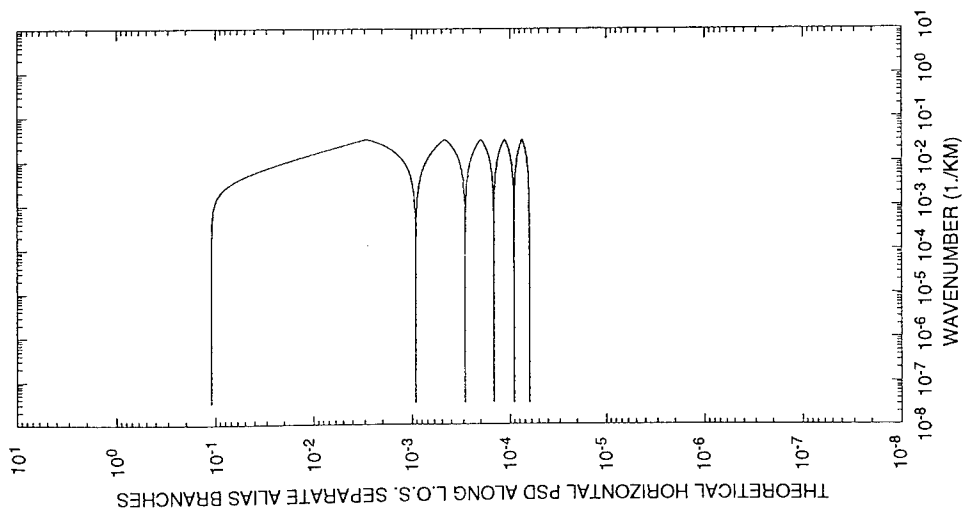


Figure A1. Alias Branches of Estimated "Theoretical" LOS PSD.

A2. RECTANGULAR WINDOW CORRECTION - TRUNCATION OF AUTOCORRELATION FUNCTION

The horizontal two-dimensional discrete Fourier Transform used in the syntheses of the database results in a well-known rectangular window sampling effect. Assuming negligible truncation of the autocorrelation function in the line-of-sight direction, truncation in the transverse direction leads to sidelobe leakage of the frequency response function of the digitized rectangular window. In the transverse direction, the effects of leakage can be computed as the convolution of the “theoretical” $PSD(k_t, k_\ell)$ with the square of the magnitude of the frequency response of a digital sinc function. The magnitude of the digital sinc function resulting from sampling N values equally spaced by Δt in the transverse direction is:

$$|H(k_t)| = \left| \Delta t \frac{\sin(\pi k_t N \Delta t)}{\sin(\pi k_t \Delta t)} \right|.$$

This means the PSD , after accounting for leakage in the transverse direction, is the digital adjusted function, $PSD_{\otimes}(k_t, k_\ell)$ where,

$$PSD_{\otimes}(k_t, k_\ell) = \frac{1}{N \Delta t} \int_{k_t - k_{NY_t}}^{k_t + k_{NY_t}} PSD(k, k_\ell) (\Delta t)^2 \frac{\sin^2[(k_t - k) \pi N \Delta t]}{\sin^2[(k_t - k) \pi \Delta t]} dk,$$

and where we assume $PSD_{\otimes}(|k_t| > k_{NY_t}, k_\ell) = 0$. Normalizing so there is no change in the total energy, that is to say σ^2 , we arrive at the “corrected” power spectral density function,

$PSD^*(k_t, k_\ell)$. The normalization is necessary because the variance of the “continuous” power spectral density differs from the variance of the “discretized” power spectral density. The normalization depends on the continuous case variance $\sigma_{t,\ell}^2$ defined by

$\sigma_{t,\ell}^2 = \int_{-k_{NY_t}}^{k_{NY_t}} PSD(k, k_\ell) dk$, and also on the discrete case variance $\sigma_{\otimes,\ell}^2$ defined by

$$\sigma_{\otimes,\ell}^2 = \frac{1}{N \Delta t} \sum_{k_t = -k_{NY_t}}^{k_{NY_t} - \frac{1}{N \Delta t}} PSD_{\otimes}(k_t, k_\ell) \text{ (with step size } \frac{1}{N \Delta t} \text{)}.$$

The "corrected" PSD then becomes:

$$PSD^*(k_t, k_\ell) = \frac{\sigma_{t,\ell}^2}{\sigma_{\otimes,\ell}^2} \times PSD_{\otimes}(k_t, k_\ell).$$

Accounting for the discretized windowing effect, the two-dimensional white noise spectrum should be multiplied by some value $A^*(k_t, k_\ell)$. Assuming negligible contribution from the truncation of the autocorrelation function in the line-of-sight direction, $A^*(k_t, k_\ell)$ is determined by:

$$A^*(k_t, k_\ell) = \sqrt{\frac{PSD^*(k_t, k_\ell)}{\Delta t \Delta \ell}},$$

where Δt is the transverse spacing and $\Delta \ell$ is the LOS spacing. Using the expression for $A^*(k_t, k_\ell)$, a computational "correction" to each LOS frequency may be made to account for the windowing effect but such computation is prohibitively intensive. Instead, the following approximate scheme was devised.

Since by construction, $\frac{1}{N\Delta t} \int_{-k_{NY_t}}^{k_{NY_t}} |H(k)|^2 dk = 1$, the convolution theorem requires

$$\sum_{k_t} \sum_{k_\ell} A^{*2}(k_t, k_\ell) = \sigma^2. \text{ Observation of } A^*(k_t, k_\ell) \text{ indicates that the major sampling effect}$$

occurs for the $PSD(k_t, k_\ell)$ at the extrema $k_t = 0$. This observation is illustrated in Figure A2 which shows a "theoretical" transverse PSD with $k_\ell = 0$ versus a 512 point PSD "corrected", as described above, for truncation of the autocorrelation function. The plot has the same input parameters previously given for 50.6 km altitude. The one-dimensional high frequency spectral slope is $(S) = -5/3$, $\sigma^2 = 8.34 \times 10^{-4}$, $L_{ch} = 32.9$ km, and the transverse spacing = 0.1 km. The plot indicates that the "corrected" PSD closely follows the "theoretical" PSD for all the discrete frequencies except the zero frequency. To avoid the time-consuming convolution integral, an approximation was developed that modified the $PSD(k_t, k_\ell)$ at $k_t = 0$. The approximation was devised from the following reasoning. We wish the variance of our simulation to equal a given value σ^2 but the actual value of the "uncorrected" simulated

variance is equal to $\sum_{k_t} \sum_{k_\ell} A^2(k_t, k_\ell)$, where $A^2 = \frac{PSD_e(k_t, k_\ell)}{\Delta t \Delta \ell}$, and where $PSD_e(k_t, k_\ell)$ is the

two-dimensional theoretical model with aliasing in the k_ℓ direction:

$$\begin{aligned}
PSD_e(k_t, k_\ell) = & PSD(k_t, k_\ell) + PSD(k_t, 2k_{NY_\ell} - k_\ell) + PSD(k_t, 2k_{NY_\ell} + k_\ell) \\
& + PSD(k_t, 4k_{NY_\ell} - k_\ell) + PSD(k_t, 4k_{NY_\ell} + k_\ell) + \dots
\end{aligned}$$

Thus, we wish to find a modified approximate value, \hat{A} , such that the theoretical variance, σ_t^2 , is: $\sigma_t^2 = \sum_{k_t} \sum_{k_\ell} \hat{A}^2(k_t, k_\ell)$. As noted, with the extrema at $k_t = 0$, we set $\hat{A}(0, k_\ell)$ by the linear interpolation relation: $\hat{A}(0, k_\ell) = gA(0, k_\ell) + (1-g)A(k_{t=1}, k_\ell)$, where $k_{t=1}$ is the first non-zero LOS frequency value and we set all other $\hat{A}(k_t, k_\ell) = A(k_t, k_\ell)$. Then it follows:

$$\sigma_t^2 = \sum_{k_\ell} \left(gA(0, k_\ell) + (1-g)A(k_{t=1}, k_\ell) \right)^2 + \sum_{k_t \neq 0} \sum_{k_\ell} A^2(k_t, k_\ell).$$

Expanding, we find a quadratic expression for g , which is:

$$\begin{aligned}
0 = & g^2 \sum_{k_\ell} \left(A^2(0, k_\ell) + A^2(k_{t=1}, k_\ell) - 2A(0, k_\ell)A(k_{t=1}, k_\ell) \right) \\
& + g \sum_{k_\ell} \left(2A(0, k_\ell)A(k_{t=1}, k_\ell) - 2A^2(k_{t=1}, k_\ell) \right) \\
& + \sum_{k_\ell} A^2(k_{t=1}, k_\ell) + \sum_{k_t \neq 0} \sum_{k_\ell} A^2(k_t, k_\ell) - \sigma_t^2.
\end{aligned}$$

Figure A3 illustrates the computation of g on a log-log plot of g versus $\frac{L_{ct}}{\Delta t}$. The plot shows a near power law relationship between g and $\frac{L_{ct}}{\Delta t}$.

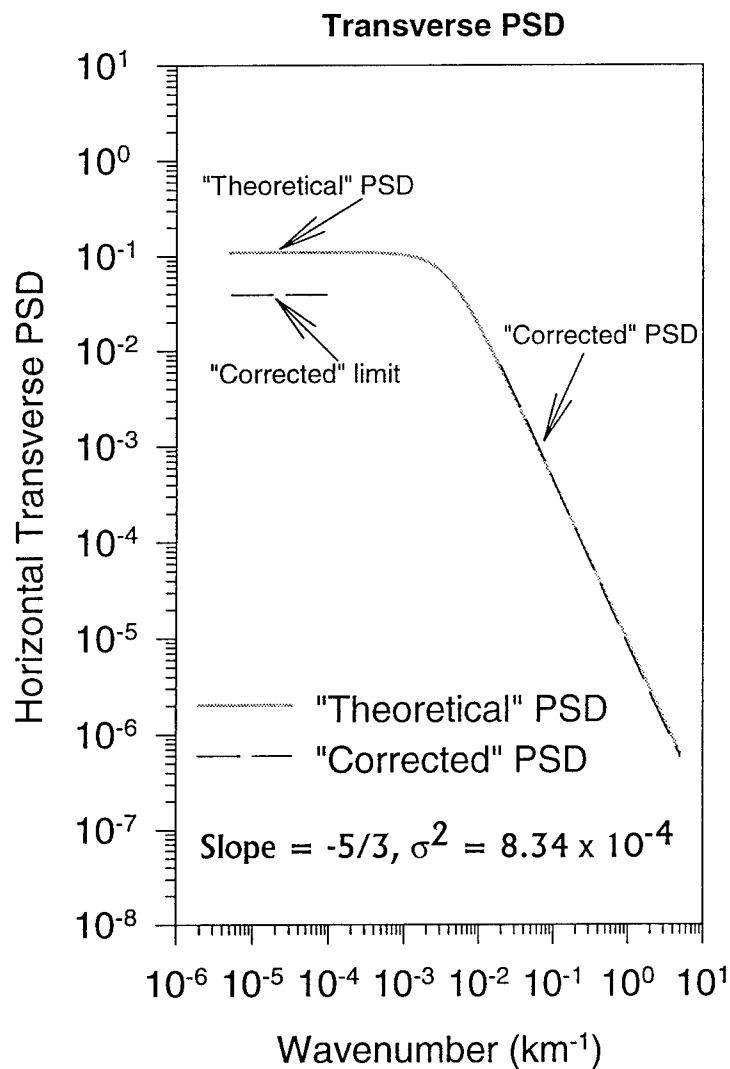


Figure A2. "Theoretical" Transverse PSD Versus a 512 Point PSD "Corrected" for Truncation of the Autocorrelation Function. The plot has the same input parameters previously given for 50.6 km altitude. The one-dimensional high frequency spectral slope is $(S) = -5/3$, $\sigma^2 = 8.34 \times 10^{-4}$, $L_{ch} = 32.9$ km and, transverse spacing = 0.1 km.

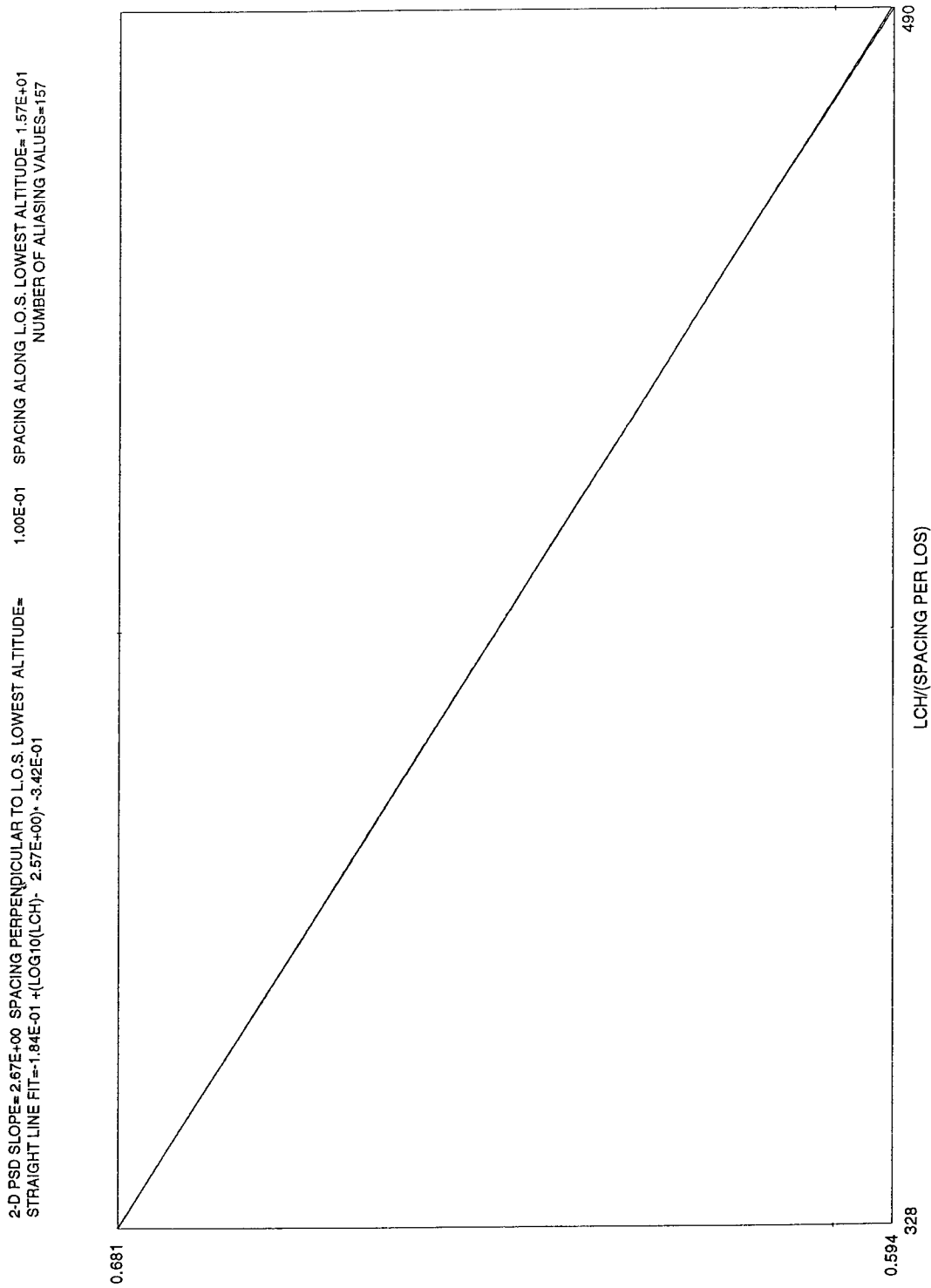


Figure A3. Approximation Correction for Rectangular Window Discrete Fourier Transform Digital Sinc Function.